Scientia Iranica B (2022) 29(2), 502–533

Sharif University of Technology
Scientia Iranica
Transactions B: Mechanical Engineering
http://scientiairanica.sharif.edu

An analytical state-space solution for free vibration of sandwich piezoelectric plate with a functionally graded core

J. Rouzegar[a,*], N. Salmanpour[a], F. Abad[a], and L. Li[b]

a. *Department of Mechanical and Aerospace Engineering, Shiraz University of Technology, Shiraz, P.O. Box 71555-313, Iran.*
b. *State Key Lab of Digital Manufacturing Equipment and Technology, School of Mechanical Science and Engineering, Huazhong University of Science and Technology, Wuhan 430074, China.*

Received 25 July 2020; received in revised form 26 June 2021; accepted 14 November 2021

KEYWORDS
State-space approach;
Free vibration;
Piezoelectric layer;
Refined plate theory;
Levy solution.

Abstract. The main objective of this study is to develop an analytical solution for free vibration analysis of smart Functionally Graded (FG) plates using Levy solution in conjunction with state-space approach. The FG substrate is sandwiched between two piezoelectric layers. The rectangular structure has two simply-supported opposite edges while the boundary conditions of the other two edges are arbitrary. Based on the simple, yet efficient, four-variable refined plate theory, the governing equations are extracted using Maxwell's equation and Hamilton's principle. The obtained fourth-order partial differential equations are transformed into the first-order ordinary ones using the Levy solution along with the state-space approach and then, they are solved through the eigenvalue method. Meanwhile, an iterative algorithm is proposed to obtain the natural frequencies of the structure under different boundary conditions. A comparison is made between the obtained results and those available in the literature which verifies the accuracy of the solution method and numerical algorithm proposed in this study. Finally, the effects of several parameters such as the type of boundary conditions, aspect ratio, power-law index, piezoelectric layer thickness, and thickness-to-side ratio on the obtained results are examined.

1. Introduction

Thin-walled structures such as beams, plates, and shells have been widely used in numerous industrial applications. This is one of the reasons why a wide range of researches have been performed on their static, dynamic, and vibration behavior [1–6]. Functionally Graded Material (FGM) is a subset of composite materials with non-homogeneous mechanical properties changing continuously in different directions. One of the typical classes of FGMs is made of ceramic and metal. Ceramic enables them to resist and tolerate high levels of heat and temperature due to their low heat transfer coefficient and high resistance to temperature. On the other hand, metal provides the required structural flexibility. Of note, owing to continuous mechanical properties in these materials, the problems of discontinuity in laminated composites are not observed in FG structures. Several plate theories have been employed to study different behaviors of Functionally Graded (FG) plate structures. Abrate [4] and Yin et

*. *Corresponding author. Tel./Fax: +9871 37264102*
E-mail address: rouzegar@sutech.ac.ir (J. Rouzegar)

doi: 10.24200/sci.2021.56480.4741

al. [5] used Classical Plate Theory (CPT), the first and simplest plate theory, for free vibration analysis of thin FG plates. Despite the simplicity of this theory, it is not desirable for analysis of thick plates since it neglects the transverse shear stresses effects. In addition, in the context of free vibration analysis, this theory is only viable for finding lower modes of natural frequencies (even for thin plates), while it encounters errors in unacceptable errors for higher modes. To overcome these problems, most of the studies on the analysis of thick FG plates have employed a type of First-order Shear Deformation Theory (FSDT). Hosseini-Hashemi et al. [7] employed the FSDT for free vibration analysis of an FG plate resting on Winkler or Pasternak elastic foundations. Thai and Choi [8] performed bending and free vibration analysis of FG plates based on the FSDT. Thai et al. [9] utilized a simple FSDT to present analytical solutions for buckling, free vibration, and bending analyses of FG sandwich plates in several boundary conditions. Anamagh and Bediz [10] used the FSDT and spectral-Chebyshev method for buckling and free vibration analysis of an FG porous plate reinforced with Graphene Platelets (GPLs). One of the main problems of the FSDT used in these researches is the violation of zero traction conditions on free surfaces. In addition, to compensate for the effect of excessive transverse shear energies, a shear correction factor is required in the FSDT formulations; however, determination of this factor is another challenge. Aiming to overcome these flaws, several researchers have utilized Higher-order Shear Deformation plate Theories (HSDTs) for different analyses of FG plate structures. Matsunaga [11] employed a two-dimensional theory and presented an analytical solution based on the Navier approach to free vibration and stability analyses of simply-supported rectangular FG plates. Baferani et al. [12] utilized the Third-order Shear Deformation plate Theory (TSDT) to address the free vibration analysis of rectangular FG plates under different Levy-type boundary conditions resting on a two-parameter elastic foundation. Ebrahimi and Heidari [13] evaluated the surface effect on the nonlinear vibration of FG nanoplates on the Pasternak foundation using the HSDT. To this end, they used Generalized Differential Quadrature (GDQ) method for solving the governing equation of the plate in different boundary conditions. Belkhodja et al. [14] studied the buckling, free vibration, and bending behavior of the simply-supported FG plates using an exponential-trigonometric HSDT and Navier method.

Due to a relatively large number of variables required in conventional HSDTs, several new and simple Refined Plate Theories (RPTs) have been introduced recently. Two-variable RPT was presented for the first time by Shimpi [15] in 2002. This efficient and simple theory, with only two unknown variables called bending and shear deflections, is well formulated for different analyses of both thick and thin plates. It can predict the quadratic distribution of transverse shear stresses through the thickness of the plate. Hence, the zero traction conditions are fulfilled on free surfaces and unlike the FSDT, there is no need to use the shear correction factor. This theory can be upgraded to the four-variable RPT by incorporating in-plane displacements in the formulation. The four-variable theory with a much simpler framework than that of the conventional HSDTs like TSDT has been widely utilized in different analyses of plate problems. Benachour et al. [16] considered this theory in the free vibration analysis of FG plates with different gradients. They used the Navier and Ritz methods to obtain a solution to the simply-supported and clamped plates, respectively. Based on an RPT as well as the Levy method, free vibration of an FG plate on an elastic foundation was addressed by Thai and Choi [17]. Hadji et al. [18] and Mechab et al. [19] concentrated on the free and forced vibration analysis of simply-supported FG plates using the RPT along with the Navier solution. Demirhan and Taskin [20] employed the state-space method to find an analytical solution based on the RPT for free vibration and bending analyses of porous FG plates. Tan et al. [21] carried out static and dynamic analyses of cracked FG plates using the two-variable refined theory and extended isogeometric analysis based on the Bézier extraction. Le et al. [22] measured the free vibration of the FG sandwich plate resting on the Pasternak foundation using the mentioned theory and finite element formulation. In all the above-mentioned researches, the formulations were established based on Equivalent Single Layer (ESL) theories. Abrate and Di Sciuva [23] conducted a review on the application of ESL theories for composite and sandwich structures. Of note, a number of researches have used layer-wise theories, such as zigzag theory, for different analyses of composite, FG, and sandwich structures [24–29].

Piezoelectric materials are a subset of smart materials. When they are exposed to mechanical deformation, an electric charge is produced on their surface which is called the direct piezoelectric effect. In addition, if an electric field is exerted on them, a mechanical strain occurs in the structure which is called the reverse piezoelectric effect. Piezoelectric materials are extensively used as actuators and sensors in different engineering and industrial applications owing to their electromechanical coupling properties, high accuracy, wide bandwidth, and quick response. Several studies have been carried out on the mechanical behavior of FG beams, plates, and panels coupled with piezoelectric layers or surface-integrated piezo-patches. He et al. [30] conducted an early study and developed a finite element formulation based on the CPT for smart FG plates. They focused on vibration and shape con-

trol of the structure using a velocity feedback control algorithm. Askari Farsangi and Saidi [31] and Askari Farsangi et al. [32] presented analytical solutions based on the Mindlin plate theory assumption for free vibration investigation of rectangular plates attached to piezoelectric layers. Alibeigloo [33] examined the free vibration of simply-supported FG Carbon Nanotube-Reinforced Composite (FG-CNTRC) cylindrical panels with a piezoelectric actuator and sensor using a three-dimensional piezo-elasticity approach. Bruant and Proslier [34] investigated the active vibration control of FGM beam with piezoelectric patches. Rouzegar and Abad [35] employed the RPT and Navier methods to measure the free vibration of FG plates bonded with the piezoelectric layers. Abad and Rouzegar [36] studied the free vibration of the Ley-type FG plates bonded with the piezoelectric layers through the spectral element method. They also used the FSDT to obtain the governing equations and suggested a closed-form solution in the frequency domain. El Harti et al. [37] proposed a finite element model for dynamic analysis of the sandwich FG Timoshenko beam integrated with Piezoelectric layers that acted as both sensor and actuator. Zhang et al. [38] focused on the static and dynamic behaviors of CNT-reinforced FG plates integrated with piezoelectric layers using a nonlinear finite element method and FSDT. Shahdadi and Rahnama [39] conducted free vibration analysis of a simply-supported FG annular sector with two piezoelectric layers based on the FSDT. To this end, they defined four functions to reformulate and decouple the governing equations and applied the harmonic motion supposition and Fourier expansion to solve them. Rouzegar and Davoudi [40] developed a finite element formulation based on the four-variable RPT for forced vibration analysis of viscoelastic composite laminates integrated with a piezoelectric actuator layer. Aghakhani et al. [41] and Motlagh et al. [42] presented an electromechanical model to investigate the dynamic behavior of FG panels and plates with multiple surface-integrated piezo-patches. The formulations were based on the Mindlin plate theory assumption, and the spectral Tchebychev technique was employed to solve the governing equations.

The state-space method is an analytical and efficient way to solve ordinary differential equations to convert higher-order differential equations into a system of first-order ones. The first-order differential equations can be easily solved by matrix methods in terms of eigenvalues and eigenvectors. Several studies have been conducted on how the state-space concept could be used for different analyses of smart plates. Chen and Ding [43] also considered the state-space technique for free vibration analysis of Functionally Graded Piezoelectric (FGP) plates. Kapuria and Achary [44] studied the steady-state response of a simply-supported cross-ply hybrid plate with piezoelectric layers based on a three-dimensional piezoelectricity theory. They expanded the parameters of Fourier series fulfilling the boundary conditions at the plate edges. Then, by replacing them with the parameters in the governing equations, the ordinary differential equations were obtained and solved through the state-space technique. Bian et al. [45] employed both state-space approach and piezoelectric theory to address the bending and free vibration of hybrid plates consisting of an FG elastic core bonded with two homogeneous piezoelectric layers acting as actuator and sensor. Yas et al. [46], Jodaei et al. [47], and Yas and Moloudi [48] extended a Differential Quadrature Method (DQM) based on the state-space concept to investigate the free vibration of annular FGP plates under different boundary conditions. A semi-analytical solution was proposed by Xin and Hu [49] for free vibration examination of multi-layer magneto-electro-elastic plates. They employed a novel hybrid method that incorporated the state-space concept as well as the discrete singular convolution algorithm. Feri et al. [50] proposed a semi-analytical solution to bending and free vibration of a cross-ply laminated plate with piezoelectric layers in arbitrary boundary conditions. They utilized the DQM in two plane directions of the plate and employed the state-space method across the thickness. Ezzin et al. [51] applied the state-space approach to assess the dynamic response and wave propagation in magneto-electro-elastic plates. Safarpour et al. [52] carried out free vibration and bending analyses of FG graphene platelet-reinforced composite truncated conical shell, cylindrical shell, and annular plate based on three-dimensional elasticity theory, DQM, and state-space approach.

According to a review of this subject, no attempt has been made to offer an analytical solution as well as the state-space approach for free vibration analysis of the smart plates based on the four-variable refined theory. The novelty of this research lies in suggesting a Levy solution in conjunction with the state-space technique for the FG plate bonded with the piezoelectric layers. Of note, no study has been reported on the application of the state-space method to solve Levy-type plates based on the RPT. Unlike most studies which were limited to simply-supported plate structures, the present study carried out the free vibration analysis of the smart FG plates under different Levy-type boundary conditions. Another contribution of the current study is application of the four-variable RPT in the present approach which is a novel, simple, and effective HSDT that can predict the parabolic distribution of transverse shear stresses through the plate thickness. Hamilton's principle and Maxwell's equation were also employed to obtain the coupled electromechanical governing differential

equations. The partial differential equations were then converted to ordinary ones in the context of the Levy solution approach. The state-space method converts higher-order ordinary differential equations into the first-order ones and then, the transfer matrix and iterative algorithm are used to determine the natural frequencies. Further, the design of an efficient iteration algorithm was proposed to obtain the natural frequencies of the studied plate. In the case of very thin plates, computer overflow/underflow may occur; therefore, a solution to such a problem should be presented. The accuracy of the proposed approach is confirmed by comparing the results with those reported by other researchers. Finally, the effects of type of boundary conditions, aspect ratio, power-law index, piezoelectric layer thickness, and thickness-to-side ratio on the natural frequencies were evaluated.

2. Theoretical formulation

2.1. Problem description and assumptions

Figure 1 shows a geometrical vision of the smart FG structure made of an FG core plate integrated with two piezoelectric layers at the bottom and top faces. In this figure, a and b indicate the plate length and width, and h_p and $2h$ are the piezoelectric layer and FG core plate thicknesses, respectively.

Based on the four-variable RPT, the displacement field is defined as:

$$u(x,y,z) = u_0(x,y) - z\frac{\partial w_b(x,y)}{\partial x} - f(z)\frac{\partial w_s(x,y)}{\partial x},$$

$$v(x,y,z) = v_0(x,y) - z\frac{\partial w_b(x,y)}{\partial y} - f(z)\frac{\partial w_s(x,y)}{\partial y},$$

$$w(x,y,z) = w_b(x,y) + w_s(x,y), \tag{1}$$

where u_0 and v_0 represent the in-plane displacements of the mid-surface along the x and y directions, respectively. The transverse displacement is split into two parts: the bending component w_b and the shear component w_s. Here, $f(z)$ is the shape function which is a third-order polynomial function [53]:

$$f(z) = -\frac{z}{4} + \frac{5z^3}{3(2h+2h_p)^2}. \tag{2}$$

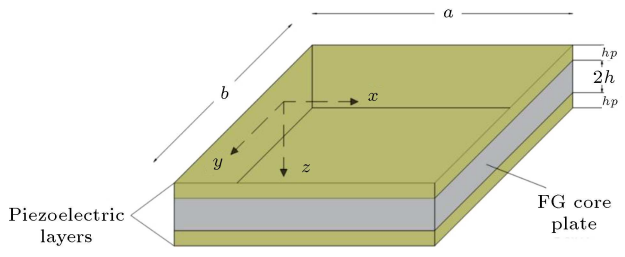

Figure 1. Geometry of a smart functionally graded plate.

As a result, the strain-displacement relationships are defined as:

$$\left\{\begin{array}{c}\varepsilon_x\\ \varepsilon_y\\ \gamma_{xy}\end{array}\right\} = \left\{\begin{array}{c}\frac{\partial u_0}{\partial x}\\ \frac{\partial v_0}{\partial y}\\ \frac{\partial u_0}{\partial y}+\frac{\partial v_0}{\partial x}\end{array}\right\} + z\left\{\begin{array}{c}-\frac{\partial^2 w_b}{\partial x^2}\\ -\frac{\partial^2 w_b}{\partial y^2}\\ -2\frac{\partial^2 w_b}{\partial x\partial y}\end{array}\right\} + f\left\{\begin{array}{c}-\frac{\partial^2 w_s}{\partial x^2}\\ -\frac{\partial^2 w_s}{\partial y^2}\\ -\frac{2\partial^2 w_s}{\partial x\partial y}\end{array}\right\},$$

$$\varepsilon_z = 0,$$

$$\left\{\begin{array}{c}\gamma_{xz}\\ \gamma_{yz}\end{array}\right\} = g\left\{\begin{array}{c}\frac{\partial w_s}{\partial x}\\ \frac{\partial w_s}{\partial y}\end{array}\right\}, \tag{3}$$

where:

$$g = 1 - \frac{df(z)}{dz} = \frac{5}{4} - 5\left(\frac{z}{2h+2h_p}\right)^2. \tag{4}$$

The coupled constitutive equations are expressed as follows [54]:

$$\{\boldsymbol{\sigma}\} = [\mathbf{C}]\{\boldsymbol{\varepsilon}\} - [\mathbf{e}]\{\boldsymbol{\Xi}\},$$

$$\{\mathbf{d}\} = [\mathbf{e}]^{\mathbf{T}}\{\boldsymbol{\varepsilon}\} + [\boldsymbol{\eta}]\{\boldsymbol{\Xi}\}, \tag{5}$$

where $\mathbf{C}$ denotes the matrix of stress-reduced stiffness; $\mathbf{d}$ and $\boldsymbol{\Xi}$ are the vectors of the electric displacement and electric field intensity, respectively; $\boldsymbol{\eta}$ is the dielectric constant matrix; $\mathbf{e}$ represents the piezoelectric constants matrix; and $\boldsymbol{\sigma}$ and $\boldsymbol{\varepsilon}$ present the stress and strain, respectively. Eq. (5) is expressed in Eq. (6), shown in Box I, for a transversely isotropic piezoelectric layer, where:

$$\bar{C}_{11} = C_{11} - \frac{C_{13}^2}{C_{33}}, \quad \bar{C}_{12} = C_{12} - \frac{C_{13}^2}{C_{33}},$$

$$\bar{e}_{31} = e_{31} - \frac{C_{13}}{C_{33}}e_{33}, \quad \overline{\eta}_{33} = \eta_{33} + \frac{e_{33}^2}{C_{33}}, \tag{7}$$

where C_{ij} denotes the components of the material matrix of the piezoelectric layer. The constitutive equation for the FG core is expressed as:

$$\left\{\begin{array}{c}\sigma_{xx}\\ \sigma_{yy}\\ \sigma_{xy}\\ \sigma_{yz}\\ \sigma_{xz}\end{array}\right\} = \left[\begin{array}{ccccc}Q_{11}&Q_{12}&0&0&0\\ Q_{12}&Q_{11}&0&0&0\\ 0&0&Q_{66}&0&0\\ 0&0&0&0&Q_{66}\\ 0&0&0&Q_{66}&0\end{array}\right] \left[\begin{array}{c}\varepsilon_{xx}\\ \varepsilon_{yy}\\ \gamma_{xy}\\ \gamma_{yz}\\ \gamma_{xz}\end{array}\right], \tag{8}$$

where:

$$\begin{Bmatrix} \sigma_{xx} \\ \sigma_{yy} \\ \sigma_{xy} \\ \sigma_{xz} \\ \sigma_{yz} \end{Bmatrix} = \begin{bmatrix} \overline{C}_{11} & \overline{C}_{12} & 0 & 0 & 0 \\ \overline{C}_{12} & \overline{C}_{11} & 0 & 0 & 0 \\ 0 & 0 & \frac{1}{2}(\overline{C}_{11} - \overline{C}_{12}) & 0 & 0 \\ 0 & 0 & 0 & C_{55} & 0 \\ 0 & 0 & 0 & 0 & C_{55} \end{bmatrix} \begin{bmatrix} \varepsilon_{xx} \\ \varepsilon_{yy} \\ \gamma_{xy} \\ \gamma_{xz} \\ \gamma_{yz} \end{bmatrix} - \begin{bmatrix} 0 & 0 & \overline{e}_{31} \\ 0 & 0 & \overline{e}_{31} \\ 0 & 0 & 0 \\ -e_{51} & 0 & 0 \\ 0 & -e_{51} & 0 \end{bmatrix} \begin{Bmatrix} \Xi_x \\ \Xi_y \\ \Xi_z \end{Bmatrix},$$

$$\begin{Bmatrix} d_x \\ d_y \\ d_z \end{Bmatrix} = \begin{bmatrix} 0 & 0 & 0 & e_{51} & 0 \\ 0 & 0 & 0 & 0 & e_{51} \\ \overline{e}_{31} & \overline{e}_{31} & 0 & 0 & 0 \end{bmatrix} \begin{Bmatrix} \varepsilon_{xx} \\ \varepsilon_{yy} \\ \gamma_{xy} \\ \gamma_{xz} \\ \gamma_{yz} \end{Bmatrix} + \begin{bmatrix} \eta_{11} & 0 & 0 \\ 0 & \eta_{11} & 0 \\ 0 & 0 & \overline{\eta}_{33} \end{bmatrix} \begin{Bmatrix} \Xi_x \\ \Xi_y \\ \Xi_z \end{Bmatrix}. \quad (6)$$

Box I

$$Q_{11} = \frac{E(z)}{1-v^2}, \quad Q_{12} = \frac{vE(z)}{(1-v^2)}, \quad Q_{66} = \frac{E(z)}{2(1+v)}, \quad (9)$$

where v and E are Poisson's ratio and modulus of elasticity, respectively. The effective properties of the FG core change according to the rule of mixture, as shown in the following relations:

$$\rho(z) = \rho_m + (\rho_c - \rho_m)\left(\frac{1}{2} - \frac{z}{2h}\right)^n, \quad (10)$$

$$E(z) = E_m + (E_c - E_m)\left(\frac{1}{2} - \frac{z}{2h}\right)^n, \quad (11)$$

where ρ is the mass density; n represents the power-law index; and c and m indicate the ceramic and metal materials, respectively. The equation related to the electric field Ξ and electric potential ϕ is introduced as:

$$\Xi_i = -\phi_{,i} \qquad i = 1, 2, 3. \quad (12)$$

Suppose that each piezoelectric layer has a closed-circuit condition; then, a quadratic function through the thickness is considered for the electric potential ϕ [55].

$$\phi(x, y, z, t) = \begin{cases} \varphi(x, y, t)\left[1 - \left(\frac{-z-h-h_p/2}{h_p/2}\right)^2\right], & -h-h_p \le z \le -h \\ \varphi(x, y, t)\left[1 - \left(\frac{z-h-h_p/2}{h_p/2}\right)^2\right], & h \le z \le h+h_p \end{cases} \quad (13)$$

2.2. Governing equations

Based on Hamilton's principle, the governing equations for the free vibration problem can be achieved as follows:

$$\int_0^t \delta(U - K) = 0, \quad (14)$$

where U and K are the strain and kinetic energies, respectively, as defined in the following:

$$U = \frac{1}{2}\int_V \sigma_{ij}\varepsilon_{ij} dV = \frac{1}{2}\int_V (\sigma_x\varepsilon_x + \sigma_y\varepsilon_y + \sigma_{xy}\gamma_{xy} + \sigma_{yz}\gamma_{yz} + \sigma_{xz}\gamma_{xz}) dV, \quad (15)$$

$$K = \frac{1}{2}\int_V \rho(z)\left[\left(\dot{u}_0 - z\frac{\partial \dot{w}_b}{\partial x} - f\frac{\partial \dot{w}_s}{\partial x}\right)^2 + \left(\dot{v}_0 - z\frac{\partial \dot{w}_b}{\partial y} - f\frac{\partial \dot{w}_s}{\partial y}\right)^2 + (\dot{w}_b + \dot{w}_s)^2\right] dV. \quad (16)$$

These over dots indicate the derivation of the parameters with respect to time. By substituting Eqs. (15) and (16) into Eq. (14), collecting the parameters of δu_0, δv_0, δw_b, and δw_s and setting them to zero, we can obtain the four following governing equations:

$$\delta u_0: \quad \frac{\partial N_x}{\partial x} + \frac{\partial N_{xy}}{\partial y} = I_0\ddot{u}_0 - I_1\frac{\partial \ddot{w}_b}{\partial x} - I_3\frac{\partial \ddot{w}_s}{\partial x}, \quad (17)$$

$$\delta v_0: \quad \frac{\partial N_y}{\partial y} + \frac{\partial N_{xy}}{\partial x} = I_0\ddot{v}_0 - I_1\frac{\partial \ddot{w}_b}{\partial y} - I_3\frac{\partial \ddot{w}_s}{\partial y}, \quad (18)$$

$$\delta w_b: \quad \frac{\partial^2 M_x^b}{\partial x^2} + \frac{\partial^2 M_y^b}{\partial y^2} + 2\frac{\partial^2 M_{xy}^b}{\partial x \partial y} = I_0(\ddot{w}_b + \ddot{w}_s) + I_1\left(\frac{\partial \ddot{u}_0}{\partial x} + \frac{\partial \ddot{v}_0}{\partial y}\right) - I_2\nabla^2\ddot{w}_b - I_4\nabla^2\ddot{w}_s, \quad (19)$$

$$\delta w_s: \quad \frac{\partial^2 M_x^s}{\partial x^2} + \frac{\partial^2 M_y^s}{\partial y^2} + 2\frac{\partial^2 M_{xy}^s}{\partial x \partial y} + \frac{\partial S_{yz}}{\partial y} + \frac{\partial S_{xz}}{\partial x} = I_0(\ddot{w}_b + \ddot{w}_s) + I_3\left(\frac{\partial \ddot{u}_0}{\partial x} + \frac{\partial \ddot{v}_0}{\partial y}\right) - I_4\nabla^2\ddot{w}_b - I_5\nabla^2\ddot{w}_s, \quad (20)$$

where I_i represents the mass moment of inertia and M, N, and S are the couple and stress resultants which are described as follows:

$$\left\{\begin{array}{c} N_x \\ N_y \\ N_{xy} \end{array}\right\} = \int_{-h-h_p}^{h+h_p} \left\{\begin{array}{c} \sigma_x \\ \sigma_y \\ \sigma_{xy} \end{array}\right\} \mathrm{d}z,$$

$$\left\{\begin{array}{c} M_x^b \\ M_y^b \\ M_{xy}^b \end{array}\right\} = \int_{-h-h_p}^{h+h_p} \left\{\begin{array}{c} \sigma_x \\ \sigma_y \\ \sigma_{xy} \end{array}\right\} z \ \mathrm{d}z,$$

$$\left\{\begin{array}{c} M_x^s \\ M_y^s \\ M_{xy}^s \end{array}\right\} = \int_{-h-h_p}^{h+h_p} \left\{\begin{array}{c} \sigma_x \\ \sigma_y \\ \sigma_{xy} \end{array}\right\} f \ \mathrm{d}z,$$

$$\left\{\begin{array}{c} S_{yz} \\ S_{xz} \end{array}\right\} = \int_{-h-h_p}^{h+h_p} \left\{\begin{array}{c} \sigma_{yz} \\ \sigma_{xz} \end{array}\right\} g \ \mathrm{d}z,$$

$$\left\{\begin{array}{c} I_0 \\ I_1 \\ I_2 \\ I_3 \\ I_4 \\ I_5 \end{array}\right\} = \int_{-h-h_p}^{h+h_p} \rho(z) \left\{\begin{array}{c} 1 \\ z \\ z^2 \\ f \\ zf \\ f^2 \end{array}\right\} \mathrm{d}z. \tag{21}$$

By substituting the stress-strain relationships, strain-displacement equations, and Eq. (21) into Eqs. (17)–(20), the governing equations of a plate can be written as follows:

$$\begin{aligned} &A_{11}\frac{\partial^2 u_0}{\partial x^2} + A_{66}\frac{\partial^2 u_0}{\partial y^2} + (A_{12}+A_{66})\frac{\partial^2 v_0}{\partial x \partial y} \\ &\quad -B_{11}\frac{\partial^3 w_b}{\partial x^3} - (B_{12}+2B_{66})\frac{\partial^3 w_b}{\partial x \partial y^2} \\ &\quad -D_{11}\frac{\partial^3 w_s}{\partial x^3} - (D_{12}+2D_{66})\frac{\partial^3 w_s}{\partial x \partial y^2} \\ &\quad = I_0 \ddot{u}_0 - I_1 \frac{\partial \ddot{w}_b}{\partial x} - I_3 \frac{\partial \ddot{w}_s}{\partial x}, \end{aligned} \tag{22}$$

$$\begin{aligned} &A_{22}\frac{\partial^2 v_0}{\partial y^2} + A_{66}\frac{\partial^2 v_0}{\partial x^2} + (A_{12}+A_{66})\frac{\partial^2 u_0}{\partial x \partial y} - B_{22}\frac{\partial^3 w_b}{\partial y^3} \\ &\quad -(B_{12}+2B_{66})\frac{\partial^3 w_b}{\partial x^2 \partial y} - D_{22}\frac{\partial^3 w_s}{\partial y^3} \\ &\quad -(D_{12}+2D_{66})\frac{\partial^3 w_s}{\partial x^2 \partial y} = I_0 \ddot{v}_0 - I_1 \frac{\partial \ddot{w}_b}{\partial y} \\ &\quad -I_3 \frac{\partial \ddot{w}_s}{\partial y}, \end{aligned} \tag{23}$$

$$\begin{aligned} &B_{11}\frac{\partial^3 u_0}{\partial x^3} + (B_{12}+2B_{66})\frac{\partial^3 u_0}{\partial x \partial y^2} + B_{22}\frac{\partial^3 v_0}{\partial y^3} \\ &\quad +(B_{12}+2B_{66})\frac{\partial^3 v_0}{\partial x^2 \partial y} - G_{11}\frac{\partial^4 w_b}{\partial x^4} \\ &\quad -(2G_{12}+4G_{66})\frac{\partial^4 w_b}{\partial x^2 \partial y^2} - G_{22}\frac{\partial^4 w_b}{\partial y^4} \\ &\quad -F_{11}\frac{\partial^4 w_s}{\partial x^4} - (2F_{12}+4F_{66})\frac{\partial^4 w_s}{\partial x^2 \partial y^2} \\ &\quad -F_{22}\frac{\partial^4 w_s}{\partial y^4} - \mu_1\left(\frac{\partial^2 \varphi}{\partial x^2} + \frac{\partial^2 \varphi}{\partial y^2}\right) = -I_2 \nabla^2 \ddot{w}_b \\ &\quad -I_4 \nabla^2 \ddot{w}_s + I_1\left(\frac{\partial \ddot{u}_0}{\partial x} + \frac{\partial \ddot{v}_0}{\partial y}\right) \\ &\quad +I_0(\ddot{w}_b + \ddot{w}_s), \end{aligned} \tag{24}$$

$$\begin{aligned} &D_{11}\frac{\partial^3 u_0}{\partial x^3} + D_{22}\frac{\partial^3 v_0}{\partial y^3} + (D_{12}+2D_{66})\frac{\partial^3 u_0}{\partial x \partial y^2} \\ &\quad +(D_{12}+2D_{66})\frac{\partial^3 v_0}{\partial x^2 \partial y} - F_{11}\frac{\partial^4 w_b}{\partial x^4} \\ &\quad -(2F_{12}+4F_{66})\frac{\partial^4 w_b}{\partial x^2 \partial y^2} - F_{22}\frac{\partial^4 w_b}{\partial y^4} \\ &\quad -H_{11}\frac{\partial^4 w_s}{\partial x^4} - (2H_{12}+4H_{66})\frac{\partial^4 w_s}{\partial x^2 \partial y^2} \\ &\quad -H_{22}\frac{\partial^4 w_s}{\partial y^4} + A_{11}^s\left(\frac{\partial^2 w_s}{\partial x^2} + \frac{\partial^2 w_s}{\partial y^2}\right) \\ &\quad +(\mu_3 - \mu_2)\left(\frac{\partial^2 \varphi}{\partial x^2} + \frac{\partial^2 \varphi}{\partial y^2}\right) \\ &\quad = I_0(\ddot{w}_b + \ddot{w}_s) + I_3\left(\frac{\partial \ddot{u}_0}{\partial x} + \frac{\partial \ddot{v}_0}{\partial y}\right) \\ &\quad -I_4 \nabla^2 \ddot{w}_b - I_5 \nabla^2 \ddot{w}_s, \end{aligned} \tag{25}$$

where:

$$\begin{aligned} \left\{\begin{array}{c} A_{1i} \\ B_{1i} \\ D_{1i} \\ G_{1i} \\ F_{1i} \\ H_{1i} \end{array}\right\} &= \int_{-h-h_p}^{-h} \bar{C}_{1i} \left\{\begin{array}{c} 1 \\ z \\ f \\ z^2 \\ zf \\ f^2 \end{array}\right\} dz \\ &\quad + \int_{-h}^{h} \bar{Q}_{1i} \left\{\begin{array}{c} 1 \\ z \\ f \\ z^2 \\ zf \\ f^2 \end{array}\right\} dz \\ &\quad + \int_{h}^{h+h_p} \bar{C}_{1i} \left\{\begin{array}{c} 1 \\ z \\ f \\ z^2 \\ zf \\ f^2 \end{array}\right\} dz, \quad i = 1, 2, \end{aligned}$$

$$\left\{\begin{array}{c} A_{66} \\ B_{66} \\ D_{66} \\ G_{66} \\ F_{66} \\ H_{66} \end{array}\right\} = \int_{-h-h_p}^{-h} \frac{1}{2}(\bar{C}_{11}-\bar{C}_{12}) \left\{\begin{array}{c} 1 \\ z \\ f \\ z^2 \\ zf \\ f^2 \end{array}\right\} \mathrm{d}z + \int_{-h}^{h} \bar{Q}_{66} \left\{\begin{array}{c} 1 \\ z \\ f \\ z^2 \\ zf \\ f^2 \end{array}\right\} \mathrm{d}z + \int_{h}^{h+h_p} \frac{1}{2}(\bar{C}_{11}-\bar{C}_{12}) \left\{\begin{array}{c} 1 \\ z \\ f \\ z^2 \\ zf \\ f^2 \end{array}\right\} \mathrm{d}z, \quad (26)$$

$$A^s{}_{11} = \int_{-h-h_p}^{-h} C_{55} g^2 \mathrm{d}z + \int_{-h}^{h} \bar{Q}_{66} g^2 \mathrm{d}z + \int_{h}^{h+h_p} C_{55} g^2 \mathrm{d}z,$$

$$\mu_1 = \frac{4}{3} e_{31} h_p, \quad \mu_2 = \frac{1}{6} \frac{h_p(8h^2+6hh_p+h_p^2)}{(h+h_p)^2} e_{31},$$

$$\mu_3 = -\frac{1}{6} \frac{h_p^2(10h+7h_p)}{(h+h_p)^2} e_{51}.$$

The following Maxwell's equation is satisfied in piezoelectric layers:

$$\int_{h}^{h+h_p} \vec{\nabla}.\ \vec{\mathbf{d}}\ dz + \int_{-h-h_p}^{-h} \vec{\nabla}.\ \vec{\mathbf{d}}\ dz = 0$$

$$\Rightarrow \int_{h}^{h+h_p} \left(\frac{\partial d_x}{\partial x} + \frac{\partial d_y}{\partial y} + \frac{\partial d_z}{\partial z}\right) dz + \int_{-h-h_p}^{-h} \left(\frac{\partial d_x}{\partial x} + \frac{\partial d_y}{\partial y} + \frac{\partial d_z}{\partial z}\right) dz = 0. \quad (27)$$

Substitution of the second relation of Eq. (6) into Eq. (27) yields:

$$\xi_1 \nabla^2 w_s - \xi_2 \nabla^2 \varphi - \xi_3 \nabla^2 w_b + \xi_4 \varphi = 0, \quad (28)$$

where:

$$\xi_1 = -\frac{(\frac{e_{31}-5e_{51}}{3})h_p^3 - \frac{h(5e_{51}-3e_{31})h_p^2}{2} + 2e_{31}h^2h_p}{(h+h_p)^2},$$

$$\xi_2 = \frac{4}{3}\eta_{11}h_p, \quad \xi_3 = 2e_{31}h_p, \quad \xi_4 = \frac{16\,\eta_{33}}{h_p}. \quad (29)$$

2.3. Boundary conditions

The plate is electrically insulated at four edges and it is characterized by simply-supported boundary conditions at $x = 0$ and $x = a$, which results in:

$$v_0 = w_s = w_b = M_x^b = M_x^s = N_x = \varphi = 0. \quad (30)$$

The boundary conditions for $y = -b/2$ and $y = +b/2$ can be arbitrarily chosen as follows:

- Simply-supported:

$$u_0 = w_s = w_b = M_y^b = M_y^s = N_y = \varphi = 0. \quad (31)$$

- Clamped:

$$u_0 = v_0 = \frac{\partial w_b}{\partial y} = \frac{\partial w_s}{\partial y} = w_b = w_s = \varphi = 0. \quad (32)$$

- Free:

$$M_y^b = M_y^s = N_y = N_{xy} = \varphi = 0,$$

$$\frac{\partial M_y^s}{\partial y} + 2\frac{\partial M_{xy}^s}{\partial x} + S_{yz} - I_3\ddot{v}_0 + I_4\frac{\partial \ddot{w}_b}{\partial y} + I_5\frac{\partial \ddot{w}_s}{\partial y} = 0,$$

$$\frac{\partial M_y^b}{\partial y} + \frac{2\partial M_{xy}^b}{\partial x} - I_1\ddot{v}_0 + I_2\frac{\partial \ddot{w}_b}{\partial y} + I_4\frac{\partial \ddot{w}_s}{\partial y} = 0. \quad (33)$$

2.4. Levy solution procedure

According to Levy solution, the forms of the following series for displacements and electrostatic potential automatically fulfil the conditions of being electrically insulated and simply supported at $x = 0$ and $x = a$:

$$\varphi(x,y,t) = \sum_{m=1}^{\infty} \varphi_m(y)\ e^{j\omega_m t} \sin\alpha x,$$

$$u_0(x,y,t) = \sum_{m=1}^{\infty} U_m(y)\ e^{j\omega_m t} \cos\alpha x,$$

$$v_0(x,y,t) = \sum_{m=1}^{\infty} V_m(y)\ e^{j\omega_m t} \sin\alpha x,$$

$$w_s(x,y,t) = \sum_{m=1}^{\infty} W_{sm}(y)\ e^{j\omega_m t} \sin\alpha x,$$

$$w_b(x,y,t) = \sum_{m=1}^{\infty} W_{bm}(y)\ e^{j\omega_m t} \sin\alpha x, \quad (34)$$

where $\alpha = \frac{m\pi}{a}$, $j = \sqrt{-1}$, ω_n the natural frequency, and $U_m(y)$, $V_m(y)$, $W_{bm}(y)$, $W_{sm}(y)$, and $\varphi_m(y)$ unknown functions. By substituting Eq. (34) into Eqs. (22)–(25) and (28), a system of ordinary differential equations can be established as follows:

$$-A_{11}\alpha^2 U_m(y) + A_{66}U''_m(y) + (A_{12}+A_{66})\,\alpha\, V'_m(y)$$
$$+B_{11}\,\alpha^3 W_{bm}(y) - (B_{12}+2B_{66})\,\alpha\, W''_{bm}(y)$$
$$+D_{11}\alpha^3 W_{sm}(y) - (D_{12}+2D_{66})\,\alpha\, W''_{sm}(y)$$
$$= -I_0{\omega_m}^2 U_m(y) + I_3{\omega_m}^2\alpha\, W_{sm}(y)$$
$$+I_1{\omega_m}^2\alpha\, W_{bm}(y)+, \quad (35)$$

$$A_{22}\, V''_m(y) - A_{66}\,\alpha^2\, V_m(y) - (A_{12}+A_{66})\,\alpha\, U'_m(y)$$
$$-B_{22}\, W'''_{bm}(y) + (B_{12}+2B_{66})\,\alpha^2\, W'_{bm}(y)$$
$$-D_{22}\, W'''_{sm}(y) + (D_{12}+2D_{66})\,\alpha^2\, W'_{sm}(y)$$
$$= -I_0{\omega_m}^2\, V_m(y) + I_1{\omega_m}^2\, W'_{bm}(y)$$
$$+I_3{\omega_m}^2\, W'_{sm}(y), \quad (36)$$

$$B_{11}\alpha^3 U_m(y) - (B_{12}+2B_{66})\,\alpha\, U''_m(y)$$
$$+B_{22}\, V'''_m(y) - (B_{12}+2B_{66})\,\alpha^2\, V'_m(y)$$
$$-G_{11}\alpha^4\, W_{bm}(y) + 2\,(G_{12}+2G_{66})\,\alpha^2\, W''_{bm}(y)$$
$$-F_{11}\alpha^4\, W_{sm}(y) + 2\,(F_{12}+2F_{66})\,\alpha^2\, W''_{sm}(y)$$
$$-G_{22}\, W''''_{bm}\,(y) - F_{22}\, W''''_{sm}\,(y)$$
$$-\mu_1\,(\varphi''_m(y) - \alpha^2\varphi_m(y)) = -I_1{\omega_m}^2(-\alpha U_m(y)$$
$$+V'_m(y)) + I_2\,{\omega_m}^2\,(-\alpha^2 W_{bm}(y) + W''_{bm}(y))$$
$$-I_0\,{\omega_m}^2(W_{bm}(y) + W_{sm}(y))$$
$$+I_4{\omega_m}^2(-\alpha^2 W_{sm}(y) + W''_{sm}(y)), \quad (37)$$

$$D_{11}\alpha^3 U_m(y) - (D_{12}+2D_{66})\,\alpha\, U''_m(y)$$
$$+D_{22}V'''_m(y) - (D_{12}+2D_{66})\,\alpha^2\, V'_m(y)$$
$$-F_{11}\alpha^4\, W_{bm}(y) + 2\,(F_{12}+2F_{66})\,\alpha^2\, W''_{bm}(y)$$
$$-F_{22}\, W''''_{bm}\,(y) - H_{11}\,\alpha^4\, W_{sm}(y)$$
$$+2\,(H_{12}+2H_{66})\,\alpha^2\, W''_{sm}(y) - H_{22}\, W''''_{sm}\,(y)$$
$$+A^s_{11}(W''_{sm}(y) - \alpha^2\, W_{sm}(y)) + (\mu_3-\mu_2)$$
$$(\varphi''_m(y) - \alpha^2\,\varphi_m(y)) = I_4{\omega_m}^2(-\alpha^2\, W_{bm}(y)$$
$$+W''_{bm}(y)) - I_0\,{\omega_m}^2(W_{bm}(y) + W_{sm}(y))$$
$$-I_3{\omega_m}^2(-\alpha\, U_m(y) + V'_m(y))$$
$$+I_5\,{\omega_m}^2(W''_{sm}(y) - \alpha^2\, W_{sm}(y)), \quad (38)$$

$$\xi_1(W''_{sm}(y) - \alpha^2\, W_{sm}(y)) - \xi_2(\varphi''_m(y) - \alpha^2\,\varphi_m(y))$$
$$-\xi_3(W''_{bm}(y) - \alpha^2\, W_{bm}(y)) + \xi_4\,\varphi_m(y) = 0, \quad (39)$$

where $()' = d/dy$. Eqs. (35)–(39) can be rearranged as follows:

$$U''_m = c_1\, U_m + c_2\, V'_m + c_3\, W_{bm} + c_4\, W''_{bm} + c_{3s}\, W_{sm}$$
$$+c_{4s}\, W''_{sm}, \quad (40)$$

$$V''_m = c_5\, U'_m + c_6\, V_m + c_7\, W'_{bm} + c_8\, W'''_{bm} + c_{7s}\, W'_{sm}$$
$$+c_{8s}\, W'''_{sm}, \quad (41)$$

$$W''''_{bm} = c_9\, U_m + c_{10}\, V'_m + c_{11}\, W_{bm} + c_{12}\, W''_{bm}$$
$$+c_{13}\, W_{sm} + c_{14}\, W''_{sm} + c_{15}\,\varphi_m, \quad (42)$$

$$W''''_{sm} = c_{9s}\, U_m + c_{10s}\, V'_m + c_{11s}\, W_{bm} + c_{12s}\, W''_{bm}$$
$$+c_{13s}\, W_{sm} + c_{14s}\, W''_{sm} + c_{15s}\,\varphi_m, \quad (43)$$

$$\varphi''_m = c_{11m}\, W_{bm} + c_{12m}\, W''_{bm} + c_{13m}\, W_{sm}$$
$$+c_{14m}\, W''_{sm} + c_{15m}\,\varphi_m. \quad (44)$$

The coefficients c_i, c_{ij}, and c_{ijm} in Eqs. (40)–(44) are given in Appendix A. The boundary conditions at $y = -b/2$ and $y = +b/2$ in terms of $U_m(y)$, $V_m(y)$, $W_{bm}(y)$, $W_{sm}(y)$, and $\varphi_m(y)$ can be written as follows:

- Simply-supported:

$$U_m(y) = W_{bm}(y) = W_{sm}(y) = \varphi_m(y) = 0,$$
$$-A_{12}\alpha\, U_m(y) + B_{12}\alpha^2\, W_{bm}(y) + D_{12}\alpha^2\, W_{sm}(y)$$
$$+A_{22}V'_m(y) - B_{22}\, W''_{bm}(y)$$
$$-D_{22}W''_{sm}(y) = 0, \quad (45)$$
$$B_{22}V'_m(y) - B_{12}\alpha\, U_m(y) + G_{12}\alpha^2\, W_{bm}(y)$$
$$-G_{22}\, W''_{bm}(y) + F_{12}\alpha^2\, W_{sm}(y)$$
$$-F_{22}\, W''_{sm}(y) - \mu_1\,\varphi_m(y) = 0,$$
$$-D_{12}\alpha\, U_m(y) + F_{12}\alpha^2\, W_{bm}(y) - F_{22}\, W''_{bm}(y)$$
$$+H_{12}\alpha^2\, W_{sm}(y) - H_{22}\, W''_{sm}(y)$$
$$+D_{22}\, V'_m(y) - \mu_2\,\varphi_m(y) = 0.$$

- Clamped:

$$U_m(y) = V_m(y) = W_{bm}(y) = W'_{bm}(y) = W_{sm}(y)$$
$$= W'_{sm}(y) = \varphi_m(y) = 0. \quad (46)$$

- Free:

$$\varphi_m = 0,$$

$$\begin{aligned}
&-A_{12}\alpha\, U_m(y) + B_{12}\alpha^2\, W_{bm}(y) - B_{22}\, W''_{bm}(y)\\
&\quad +D_{12}\,\alpha^2\, W_{sm}(y) - D_{22}\, W''_{sm}(y)\\
&\quad +A_{22}V'_m(y) = 0,\\
&-2D_{66}\alpha\, W'_{sm}(y) + A_{66}(U'_m(y) + \alpha\, V_m(y))\\
&\quad -2B_{66}\,\alpha\, W'_{bm}(y) = 0,\\
&B_{22}\, V'_m(y) - B_{12}\alpha\, U_m(y) + G_{12}\alpha^2\, W_{bm}(y)\\
&\quad -G_{22}\, W''_{bm}(y) + F_{12}\,\alpha^2 W_{sm}(y)\\
&\quad -F_{22}\, W''_{sm}(y) - \mu_1\,\varphi_m(y) = 0,\\
&-D_{12}\alpha\, U_m(y) + F_{12}\,\alpha^2\, W_{bm}(y) + H_{12}\alpha^2\, W_{sm}(y)\\
&\quad +D_{22}V'_m(y) - F_{22}\, W''_{bm}(y)\\
&\quad -H_{22}W''_{sm}(y) = 0.
\end{aligned} \tag{47}$$

2.5. State-space approach

Based on the state-space concept, Eqs. (40)–(44) are re-written as follows:

$$\{\mathbf{Z}'(y)\} = [\mathbf{T}]\,\{\mathbf{Z}(y)\}, \tag{48}$$

where the state vector $\mathbf{Z}(y)$ and transfer matrix $\mathbf{T}$ are defined as:

$$\begin{aligned}
\{\mathbf{Z}(y)\} = \{&U_m\ \ U'_m\ \ V_m\ \ V'_m\ \ \varphi_m\ \ \varphi'_m\ \ W_{bm}\ \ W'_{bm}\\
&W''_{bm}\ \ W'''_{bm}\ \ W_{sm}\ \ W'_{sm}\ \ W''_{sm}\ \ W'''_{sm}\}^T.
\end{aligned} \tag{49}$$

Eq. (50) is shown in Box II. The solution of Eq. (48) can be obtained as [56]:

$$\{\mathbf{Z}(y)\} = e^{Ty}\,\{\mathbf{k}\}, \tag{51}$$

where:

$$e^{Ty} = [\mathbf{X}]\begin{bmatrix} e^{\lambda_1 y} & & 0\\ & \ddots & \\ 0 & & e^{\lambda_{14} y}\end{bmatrix}[\mathbf{X}]^{-1}, \tag{52}$$

where λ_i and $\mathbf{X}$ denote the distinct eigenvalues and eigenvector of the matrix $\mathbf{T}$, respectively; further, $\mathbf{X}^{-1}$ is the reverse of $\mathbf{X}$ and $\mathbf{k}$ is a constant vector identified by applying conditions of $y = -b/2$ and $y = +b/2$. To avoid facing an ill-conditioned problem, Eq. (51) is rewritten as follows:

$$\{\mathbf{Z}(y)\} = [\mathbf{X}]\begin{bmatrix} e^{\lambda_1 y} & & 0\\ & \ddots & \\ 0 & & e^{\lambda_{14} y}\end{bmatrix}\{\mathbf{P}\}, \tag{53}$$

where:

$$\{\mathbf{P}\} = [\mathbf{X}]^{-1}\,\{\mathbf{k}\}. \tag{54}$$

At edges $y = -b/2$ and $y = +b/2$, the boundary conditions are written in terms of the state vector in the following matrix form:

$$[\hat{\mathbf{a}}]\,\{\mathbf{Z}\} = \{\mathbf{0}\}. \tag{55}$$

This matrix equation under different boundary conditions can be expressed as follows:

- Simply-supported:

Eq. (56) is shown in Box III.

- Clamped:

$$[\mathbf{T}] = \begin{bmatrix}
0 & 1 & 0 & 0 & 0 & 0 & 0 & 0 & 0 & 0 & 0 & 0 & 0 & 0\\
c_1 & 0 & 0 & c_2 & 0 & 0 & c_3 & 0 & c_4 & 0 & c_{3s} & 0 & c_{4s} & 0\\
0 & 0 & 0 & 1 & 0 & 0 & 0 & 0 & 0 & 0 & 0 & 0 & 0 & 0\\
0 & c_5 & c_6 & 0 & 0 & 0 & 0 & c_7 & 0 & c_8 & 0 & c_{7s} & 0 & c_{8s}\\
0 & 0 & 0 & 0 & 0 & 1 & 0 & 0 & 0 & 0 & 0 & 0 & 0 & 0\\
0 & 0 & 0 & 0 & c_{15m} & 0 & c_{11m} & 0 & c_{12m} & 0 & c_{13m} & 0 & c_{14m} & 0\\
0 & 0 & 0 & 0 & 0 & 0 & 0 & 1 & 0 & 0 & 0 & 0 & 0 & 0\\
0 & 0 & 0 & 0 & 0 & 0 & 0 & 0 & 1 & 0 & 0 & 0 & 0 & 0\\
0 & 0 & 0 & 0 & 0 & 0 & 0 & 0 & 0 & 1 & 0 & 0 & 0 & 0\\
c_9 & 0 & 0 & c_{10} & c_{15} & 0 & c_{11} & 0 & c_{12} & 0 & c_{13} & 0 & c_{14} & 0\\
0 & 0 & 0 & 0 & 0 & 0 & 0 & 0 & 0 & 0 & 0 & 1 & 0 & 0\\
0 & 0 & 0 & 0 & 0 & 0 & 0 & 0 & 0 & 0 & 0 & 0 & 1 & 0\\
0 & 0 & 0 & 0 & 0 & 0 & 0 & 0 & 0 & 0 & 0 & 0 & 0 & 1\\
c_{9s} & 0 & 0 & c_{10s} & c_{15s} & 0 & c_{11s} & 0 & c_{12s} & 0 & c_{13s} & 0 & c_{14s} & 0
\end{bmatrix} \tag{50}$$

Box II

$$\begin{array}{c} u_0 = 0: \\ w_b = 0: \\ w_s = 0: \\ \varphi = 0: \\ N_y = 0: \\ M_y^b = 0: \\ M_y^s = 0: \end{array} \begin{bmatrix} 1 & 0 & 0 & 0 & 0 & 0 & 0 & 0 & 0 & 0 & 0 & 0 & 0 & 0 \\ 0 & 0 & 0 & 0 & 0 & 0 & 1 & 0 & 0 & 0 & 0 & 0 & 0 & 0 \\ 0 & 0 & 0 & 0 & 0 & 0 & 0 & 0 & 0 & 0 & 1 & 0 & 0 & 0 \\ 0 & 0 & 0 & 0 & 1 & 0 & 0 & 0 & 0 & 0 & 0 & 0 & 0 & 0 \\ -A_{12}\alpha & 0 & 0 & A_{22} & 0 & 0 & B_{12}\alpha^2 & 0 & -B_{22} & 0 & D_{12}\alpha^2 & 0 & -D_{22} & 0 \\ -B_{12}\alpha & 0 & 0 & B_{22} & -\mu_1 & 0 & G_{12}\alpha^2 & 0 & -G_{22} & 0 & F_{12}\alpha^2 & 0 & -F_{22} & 0 \\ -D_{12}\alpha & 0 & 0 & D_{22} & -\mu_2 & 0 & F_{12}\alpha^2 & 0 & -F_{22} & 0 & H_{12}\alpha^2 & 0 & -H_{22} & 0 \end{bmatrix} \{\mathbf{Z}\} = \{\mathbf{0}\}. \quad (56)$$

Box III

$$\begin{array}{c} u_0 = 0: \\ v_0 = 0: \\ w_b = 0: \\ w_s = 0: \\ \frac{\partial w_b}{\partial y} = 0: \\ \frac{\partial w_s}{\partial y} = 0: \\ \varphi = 0: \end{array} \begin{bmatrix} 1 & 0 & 0 & 0 & 0 & 0 & 0 & 0 & 0 & 0 & 0 & 0 & 0 & 0 \\ 0 & 0 & 1 & 0 & 0 & 0 & 0 & 0 & 0 & 0 & 0 & 0 & 0 & 0 \\ 0 & 0 & 0 & 0 & 0 & 0 & 1 & 0 & 0 & 0 & 0 & 0 & 0 & 0 \\ 0 & 0 & 0 & 0 & 0 & 0 & 0 & 0 & 0 & 0 & 1 & 0 & 0 & 0 \\ 0 & 0 & 0 & 0 & 0 & 0 & 0 & 1 & 0 & 0 & 0 & 0 & 0 & 0 \\ 0 & 0 & 0 & 0 & 0 & 0 & 0 & 0 & 0 & 0 & 0 & 1 & 0 & 0 \\ 0 & 0 & 0 & 0 & 1 & 0 & 0 & 0 & 0 & 0 & 0 & 0 & 0 & 0 \end{bmatrix} \{\mathbf{Z}\} = \{\mathbf{0}\}. \quad (57)$$

Box IV

Eq. (57) is shown in Box IV.

- Free:

Eq. (58) is shown in Box V. Coefficients ℓ_i and ℓ_{ij} are presented in Appendix B. If we substitute the state vector $\mathbf{Z}$ from Eq. (53) into Eq. (55), the following matrix equation can be obtained:

$$[\mathrm{l}]\{\mathbf{P}\} = \{\mathbf{0}\}, \quad (59)$$

where:

$$[\mathrm{l}] = [\hat{\mathbf{a}}][\mathbf{X}] \begin{bmatrix} e^{\lambda_1 y} & & 0 \\ & \ddots & \\ 0 & & e^{\lambda_{14} y} \end{bmatrix}. \quad (60)$$

In accordance with different conditions at edges $y = -b/2$ and $y = +b/2$, replacing $\hat{\mathbf{a}}$ would yield two matrix equations. By combining these two equations, the following equation can be obtained:

$$\begin{bmatrix} [\mathrm{l}]_{y=-b/2} \\ \hline [\mathrm{l}]_{y=+b/2} \end{bmatrix} \{\mathbf{P}\} = [\mathbf{L}]\{\mathbf{P}\} = \{\mathbf{0}\}, \quad (61)$$

$$\begin{array}{c} N_y = 0: \\ N_{xy} = 0: \\ M_y^b = 0: \\ M_y^s = 0: \\ \frac{\partial M_y^b}{\partial y} + 2\frac{\partial M_{xy}^b}{\partial x} - I_1\ddot{v} + I_2\frac{\partial \ddot{w}_b}{\partial y} + I_4\frac{\partial \ddot{w}_s}{\partial y} = 0: \\ \frac{\partial M_y^s}{\partial y} + 2\frac{\partial M_{xy}^s}{\partial x} + S_{yz} - I_3\ddot{v} + I_4\frac{\partial \ddot{w}_b}{\partial y} + I_5\frac{\partial \ddot{w}_s}{\partial y} = 0: \\ \varphi = 0: \end{array} \begin{bmatrix} -A_{12}\alpha & 0 & 0 & A_{22} & 0 \\ 0 & A_{66} & A_{66}\alpha & 0 & 0 \\ -B_{12}\alpha & 0 & 0 & B_{22} & -\mu_1 \\ -D_{12}\alpha & 0 & 0 & D_{22} & 0 \\ 0 & \ell_1 & \ell_2 & 0 & 0 \\ 0 & \ell_8 & \ell_9 & 0 & 0 \\ 0 & 0 & 0 & 0 & 1 \end{bmatrix}$$

$$\begin{bmatrix} 0 & B_{12}\alpha^2 & 0 & -B_{22} & 0 & D_{12}\alpha^2 & 0 & -D_{22} & 0 \\ 0 & 0 & -2B_{66}\alpha & 0 & 0 & 0 & -2D_{66}\alpha & 0 & 0 \\ 0 & G_{12}\alpha^2 & 0 & -G_{22} & 0 & F_{12}\alpha^2 & 0 & -F_{22} & 0 \\ 0 & F_{12}\alpha^2 & 0 & -F_{22} & 0 & H_{12}\alpha^2 & 0 & -H_{22} & 0 \\ \ell_7 & 0 & \ell_3 & 0 & \ell_5 & 0 & \ell_4 & 0 & \ell_6 \\ \ell_{14} & 0 & \ell_{10} & 0 & \ell_{12} & 0 & \ell_{11} & 0 & \ell_{13} \\ 0 & 0 & 0 & 0 & 0 & 0 & 0 & 0 & 0 \end{bmatrix} \{\mathbf{Z}\} = \{\mathbf{0}\}. \quad (58)$$

Box V

which is a homogeneous equation system. To obtain a non-trivial solution with regard to natural frequency ω_m^2 associated with the nth mode, the determinant of the coefficient matrix $\mathbf{L}$ should be zero. However, since matrix $\mathbf{T}$ contains an unknown parameter ω_m^2, such a process will not directly result in the natural frequency for the plate and a trial-and-error procedure should be taken into consideration. In this study, the following iterative algorithm was employed to find the natural frequency:

1. Consider a small value for the natural frequency as an initial value;
2. After inserting the corresponding value for the natural frequency into matrix $\mathbf{T}$, calculate the eigenvalues λ_i and eigenvectors $\mathbf{X}$ of matrix $\mathbf{T}$;
3. Generate matrix $\mathbf{L}$ according to the proper form of the boundary conditions introduced in Eqs. (56)–(58);
4. Check the sign of the determinant:
   a) If there is no change in the sign of the determinant, add a certain amount to the value of natural frequency and return to Step 2 and repeat the next steps;
   b) In the case of a change in the sign, reduce the value of the frequency by a finite level and proceed to the next stage.
5. If the difference between the values of two consecutive iterations is less than a specified amount, the procedure is complete. Otherwise, return to Step 2.

The convergence criterion in this research is considered as:

$$\left(\left| \frac{\omega_{n+1} - \omega_n}{\left(\frac{\omega_{n+1}+\omega_n}{2}\right)} \right| < 10^{-4} \right).$$

The number of iterations varies for problems, but for the solved problems in this research, it changes between 170 and 3000. Example 3 reports the required number of iterations for several cases.

The flow diagram of this algorithm is shown in Figure 2. Of note, in the case of very thin plates, computer overflow/underflow may occur when calculating the elements of matrix $\mathbf{L}$. Refer to Appendix C for more details on how to solve this problem.

3. Results and discussion

Three numerical examples were solved to validate the precision and efficiency of the proposed technique. The mechanical boundary conditions of the structure are denoted by SXSY where S is the simply supported at $x = 0$ and $x = a$ and X and Y indicate conditions at $y = -b/2$ and $y = +b/2$, respectively. For example, SFSC condition is related to a plate with simply-supported, free, simply-supported, and clamped edges. The electrical boundary conditions of the surfaces of the piezoelectric layer are assumed to be closed circuit. Table 1 presents the material properties considered in these examples [31]. The non-dimensional natural frequency parameter is expressed as follows:

Table 1. Material properties [31].

	Piezoelectric layer	Core plate	
Property	**PZT-4**	**Al_2O_3**	**Al**
E (GPa)	–	380	70
υ	–	0.3	0.3
C_{11} (GPa)	132	–	–
C_{12} (GPa)	71	–	–
C_{33} (GPa)	115	–	–
C_{13} (GPa)	73	–	–
C_{55} (GPa)	26	–	–
e_{31} (cm^{-2})	–4.1	–	–
e_{33} (cm^{-2})	14.1	–	–
e_{15} (cm^{-2})	10.5	–	–
η_{11} (nFm^{-1})	7.124	–	–
η_{33} (nFm^{-1})	5.841	–	–
ρ (kgm^{-3})	7500	3800	2707

$$\bar{\omega} = \omega h \sqrt{\rho_m / E_m}. \tag{62}$$

Example 1. Consider a square FG plate that is made of 'Al/Al_2O_3'. The non-dimensional fundamental natural frequency of the structure with different thickness-to-side ratios, boundary conditions, and power-law indices was obtained and compared with the existing three-dimensional (3D) exact solution [57] in Table 2. In the fully simply-supported case, the results were also compared with those of 2D HSDT and quasi-3D HSDT [58]. As observed in the simply-supported case, despite the more complexity of HSDT with five unknown variables than the present four-variable RPT, the current approach outperformed the exact solution mainly because the error for the HSDT reached 2.28% particularly for moderately thick and thick plates ($h/a = 0.1$ and 0.2), while the maximum error in the current theory was 0.53%. The results under the other conditions are more acceptable than those of the exact solution, even for the thick plate ($h/a = 0.5$). Therefore, the present approach, in addition to its simplicity, has good accuracy while analyzing both thin and thick FG plates. Further, the good agreement between the present analytical solution and results from the exact solution is indicative of the accuracy

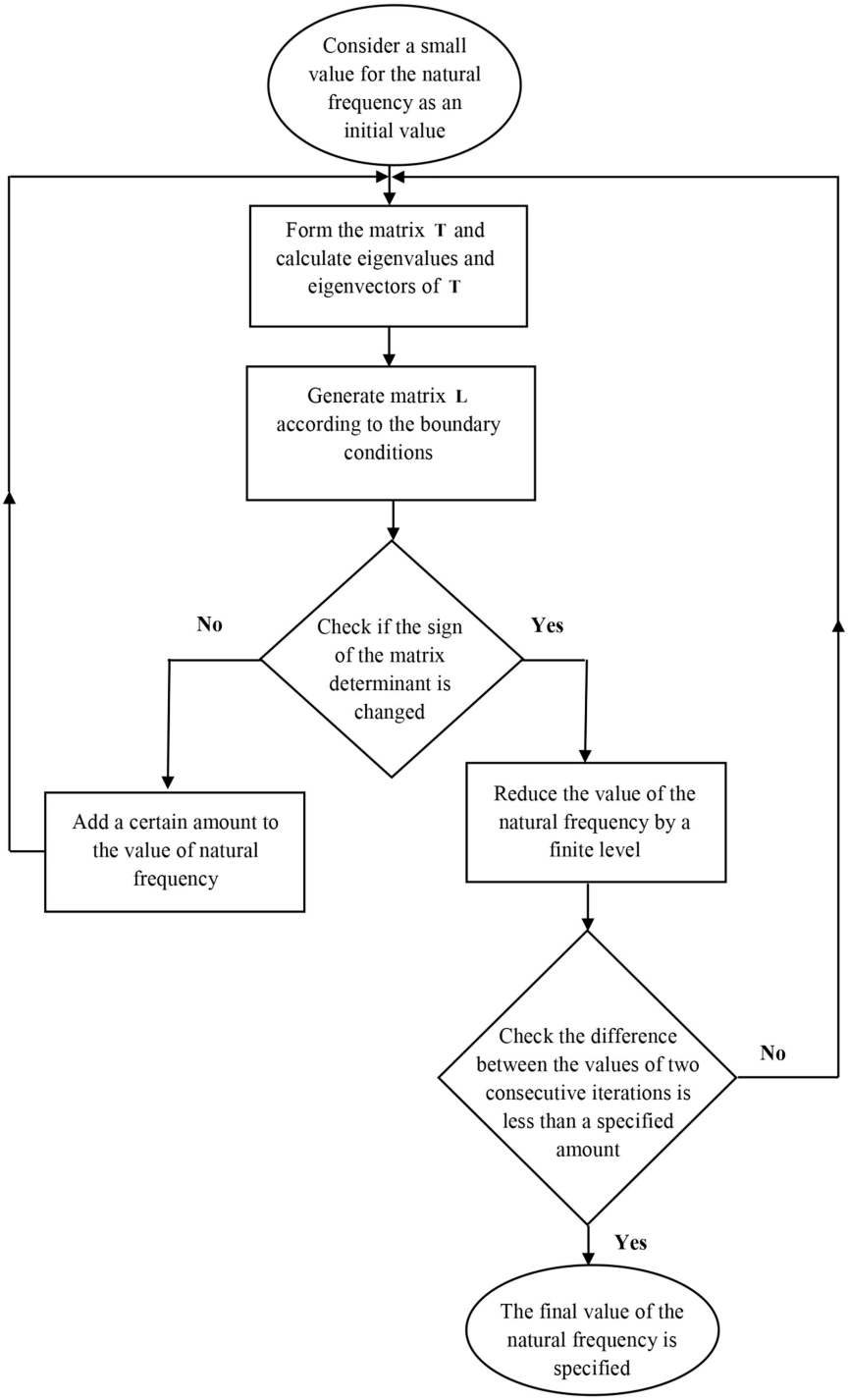

Figure 2. Flow diagram for finding the natural frequency value.

and efficiency of the state-space Levy type solution as well as the iteration algorithm.

Figure 3 indicates the variations in the non-dimensional natural frequency parameter of an FG plate in terms of the power-law index (n) with different aspect ratios (a/b). The plate is characterized by an SFSC boundary condition and $a/h = 10$. According to Figure 3, as the aspect ratio increases, the non-dimensional natural frequency increases, as well. Given that the plate length (a) is kept constant, upon increasing a/b, the plate width (b) decreases. In addition, with a decrease in the plate dimension, the plate stiffness increases, the plate mass decreases, and consequently, the natural frequency increases. Moreover, since the value of elastic modulus for 'Al' is lower than that of 'Al_2O_3', with an increase in the power-law index

Table 2. The fundamental frequency parameter ($\bar{\omega}$) of the square Functionally Graded (FG) plate.

			Power-law index			
h/a	B.Cs.	Theory	0	1	2	5
0.1	SSSS	Present	0.1133 [0.18]	0.0868 [0.23]	0.0788 [0.13]	0.0740 [0.13]
		HSDT(2D) [58]	0.1134 [0.09]	0.0868 [0.23]	0.0788 [0.13]	0.0740 [0.13]
		HSDT(quasi-3D) [58]	0.1137 [0.18]	0.0883 [1.49]	0.0807 [2.28]	0.0756 [2.02]
		Exact [57]	0.1135	0.0870	0.0789	0.0741
	SCSC	Present	0.1616 [0.75]	0.1243 [0.57]	0.1126 [0.71]	0.1049 [1.06]
		Exact [57]	0.1604	0.1236	0.1118	0.1038
	SFSF	Present	0.0563 [0.18]	0.0430 [0.00]	0.0391 [0.26]	0.0369 [0.27]
		Exact [57]	0.0562	0.0430	0.0390	0.0368
	SCSF	Present	0.0737 [0.82]	0.0564 [0.89]	0.0512 [0.99]	0.0483 [1.26]
		Exact [57]	0.0731	0.0559	0.0507	0.0477
	SSSC	Present	0.1343 [0.30]	0.1030 [0.10]	0.0934 [0.21]	0.0875 [0.46]
		Exact [57]	0.1339	0.1029	0.0932	0.0871
	SSSF	Present	0.0680 [0.44]	0.0520 [0.39]	0.0472 [0.42]	0.0445 [0.45]
		Exact [57]	0.0677	0.0518	0.0470	0.0443
0.2	SSSS	Present	0.4150 [0.45]	0.3205 [0.53]	0.2892 [0.45]	0.2667 [0.34]
		HSDT(2D) [58]	0.4151 [0.43]	0.3205 [0.53]	0.2892 [0.45]	0.2665 [0.41]
		HSDT(quasi-3D) [58]	0.4178 [0.22]	0.3267 [1.40]	0.2968 [2.17]	0.2725 [1.83]
		Exact [57]	0.4169	0.3222	0.2905	0.2676
	SCSC	Present	0.5588 [3.44]	0.4362 [2.97]	0.3923 [3.26]	0.3546 [3.92]
		Exact [57]	0.5402	0.4236	0.3799	0.3412
	SFSF	Present	0.2148 [0.33]	0.1649 [0.24]	0.1493 [0.34]	0.1394 [0.43]
		Exact [57]	0.2141	0.1645	0.1488	0.1388
	SCSF	Present	0.2772 [2.17]	0.2133 [1.96]	0.1929 [2.12]	0.1793 [2.52]
		Exact [57]	0.2713	0.2092	0.1889	0.1749
	SSSC	Present	0.4807 [1.61]	0.3728 [1.28]	0.3359 [1.48]	0.3073 [1.96]
		Exact [57]	0.4731	0.3681	0.3310	0.3014
	SSSF	Present	0.2576 [1.02]	0.1979 [0.87]	0.1791 [1.01]	0.1668 [1.15]
		Exact [57]	0.2550	0.1962	0.1773	0.1649

Table 2. The fundamental frequency parameter ($\bar{\omega}$) of the square Functionally Graded (FG) plate (continued).

			Power-law index			
h/a	B.Cs.	Theory	0	1	2	5
0.5	SSSS	Present	1.8266	1.4452	1.2890	1.1317
			[1.10]	[1.60]	[1.56]	[1.16]
		HSDT(2D) [58]	1.8287	1.4467	1.2901	1.1310
			[0.99]	[1.50]	[1.48]	[1.22]
		HSDT(quasi-3D) [58]	1.8583	1.4830	1.3269	1.1576
			[0.61]	[0.97]	[1.33]	[1.10]
		Exact [57]	1.8470	1.4687	1.3095	1.1450
	SCSC	Present	1.9139	1.5922	1.4386	1.2429
			[0.00]	[1.26]	[2.57]	[2.96]
		Exact [57]	1.9139	1.5724	1.4026	1.2072
	SFSF	Present	1.0679	0.8347	0.7479	0.6715
			[0.25]	[0.06]	[0.20]	[0.42]
		Exact [57]	1.0652	0.8342	0.7464	0.6687
	SCSF	Present	0.9671	0.8139	0.7306	0.6357
			[1.05]	[2.54]	[2.20]	[3.06]
		Exact [57]	0.9570	0.7937	0.7149	0.6168
	SSSC	Present	1.9139	1.5922	1.4217	1.2323
			[0.00]	[2.73]	[3.05]	[3.03]
		Exact [57]	1.9139	1.5499	1.3796	1.1961
	SSSF	Present	0.9680	0.8156	0.7335	0.6370
			[1.15]	[2.76]	[2.60]	[3.27]
		Exact [57]	0.9570	0.7937	0.7149	0.6168

[%Error]=(Calculated value-Exact value)/Exact value*100

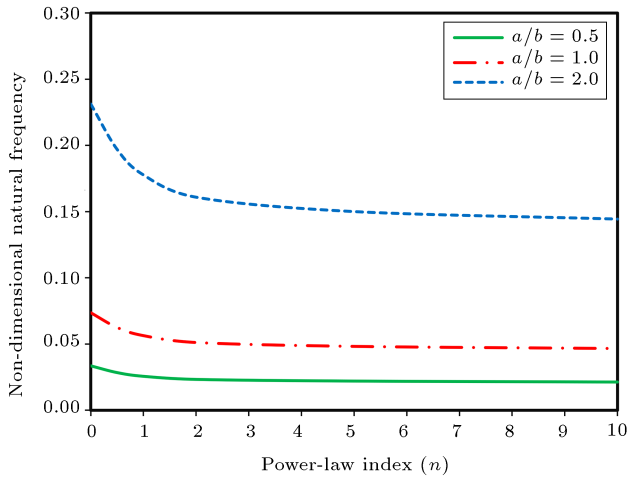

Figure 3. Non-dimensional natural frequency ($\bar{\omega}$) of Functionally Graded (FG) plates versus power-law index considering different aspect ratios (SFSC, $a/h = 10$).

(n), the stiffness and natural frequency of the plate decrease. The decrease in the rate of natural frequency slows down for n values larger than 2.

Example 2. A rectangular transversely isotropic core plate sandwiched between two PZT-4 layers on the upper and lower surfaces was taken into account. The core plate is characterized by the following material properties [32]:

$$C_{11} = 460.2 \text{ GPa}, \quad C_{12} = 174.7 \text{ GPa},$$
$$C_{33} = 509.5 \text{ GPa}, \quad C_{13} = 127.4 \text{ GPa},$$
$$C_{55} = 126.9 \text{ GPa}, \quad \rho = 4000 \text{ kg/m}^3. \tag{63}$$

Table 3 compares the three consecutive natural frequencies with those obtained by Askari Farsangi et al. [32]. In all cases, the obtained natural frequencies match properly with the FSDT results. It should be noticed that the RPT contains only four variables rather than five variables in the FSDT. In addition, the present theory fulfils the condition of zero shear stress on free surfaces that, unlike the FSDT, does not need the shear correction factor. It can be concluded that the RPT is not only precise but also simple and efficient. According to this table, upon increasing the b/a ratio, the natural frequency decreases.

Figure 4 depicts the variations in the first natural frequency of the SSSS smart plate versus the piezoelectric layer thickness, considering different thickness-to-side ratios. Given that the plate length is kept

Table 3. Three consecutive natural frequencies (Hz) of the smart transversely isotropic plate ($h_p/2h = 0.1$).

B.Cs.	$\frac{b}{a}$	$\frac{2h}{a}$	Theory	Mode numbers		
				1st	2nd	3rd
SSSF	1	0.05	Present	249.929 [0.44]	589.434 [0.84]	868.868 [0.40]
			FSDT [32]	248.830	584.511	865.376
		0.1	Present	489.709 [0.90]	1126.034 [1.67]	1626.920 [0.84]
			FSDT [32]	485.305	1107.449	1613.274
	2	0.05	Present	221.258 [0.18]	316.337 [0.34]	503.755 [0.45]
			FSDT [32]	220.847	315.254	501.467
		0.1	Present	434.434 [0.40]	616.521 [0.71]	967.966 [0.93]
			FSDT [32]	432.688	612.130	958.963
SSSS	1	0.05	Present	423.125 [0.03]	1039.337 [0.08]	1635.182 [0.12]
			FSDT [32]	422.966	1038.436	1633.073
		0.1	Present	817.591 [0.12]	1923.402 [0.24]	2919.583 [0.31]
			FSDT [32]	816.534	1918.659	2910.463
	2	0.05	Present	265.656 [0.02]	423.125 [0.03]	682.479 [0.05]
			FSDT [32]	265.592	422.966	682.077
		0.1	Present	519.668 [0.08]	817.591 [0.12]	1293.837 [0.18]
			FSDT [32]	519.218	816.537	1291.421
SCSC	1	0.05	Present	614.543 [0.80]	1147.541 [0.72]	1432.249 [1.16]
			FSDT [32]	609.652	1139.314	1415.781
		0.1	Present	1158.100 [2.65]	2101.099 [1.99]	2542.414 [3.51]
			FSDT [32]	1128.191	2060.096	2456.099
	2	0.05	Present	294.329 [0.20]	505.014 [0.39]	818.029 [0.49]
			FSDT [32]	293.724	503.042	814.007
		0.1	Present	573.770 [0.72]	966.450 [1.33]	1526.769 [1.60]
			FSDT [32]	569.657	953.729	1502.638
SFSF	1	0.05	Present	206.636 [0.21]	342.283 [1.27]	774.409 [1.44]
			FSDT [32]	206.189	337.986	763.342
		0.1	Present	406.223 [0.45]	666.318 [2.54]	1461.310 [2.80]
			FSDT [32]	404.375	649.789	1421.432
	2	0.05	Present	209.330 [0.14]	249.929 [0.44]	377.110 [0.74]
			FSDT [32]	209.027	248.830	374.330
		0.1	Present	411.398 [0.32]	489.709 [0.90]	731.808 [1.49]
			FSDT [32]	410.083	485.305	721.037

Table 3. Three consecutive natural frequencies (Hz) of the smart transversely isotropic plate ($h_p/2h = 0.1$) (continued).

B.Cs.	$\frac{b}{a}$	$\frac{2h}{a}$	Theory	Mode numbers		
				1st	2nd	3rd
SFSC	1	0.05	Present	270.811 [0.70]	699.104 [1.26]	878.835 [0.50]
			FSDT [32]	268.928	690.400	874.395
		0.1	Present	529.350 [1.58]	1319.022 [3.05]	1644.097 [1.09]
			FSDT [32]	521.069	1279.972	1626.329
	2	0.05	Present	223.859 [0.22]	337.140 [0.49]	548.998 [0.64]
			FSDT [32]	223.354	335.483	545.498
		0.1	Present	439.417 [0.50]	655.533 [1.16]	1049.464 [1.54]
			FSDT [32]	437.198	647.963	1033.508
SSSC	1	0.05	Present	505.014 [0.39]	1086.227 [0.33]	1224.056 [0.56]
			FSDT [32]	503.042	1082.550	1217.137
		0.1	Present	966.450 [1.33]	2001.302 [0.96]	2219.836 [1.74]
			FSDT [32]	953.725	1982.268	2181.779
	2	0.05	Present	278.035 [0.09]	460.833 [0.19]	746.978 [0.26]
			FSDT [32]	277.770	459.928	744.988
		0.1	Present	543.114 [0.33]	886.602 [0.67]	1405.818 [0.87]
			FSDT [32]	541.275	880.650	1393.625

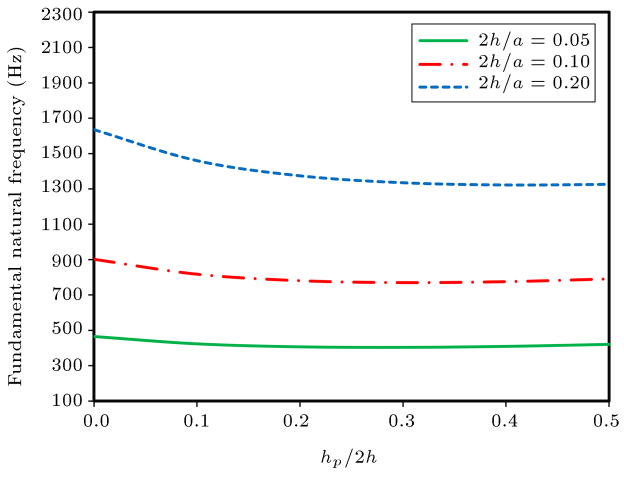

Figure 4. First natural frequency of the smart transversely isotropic plate versus piezoelectric layer thickness considering different thickness-to-side ratios.

constant, upon increasing $(2h/a)$, the plate thickness increases. The plate stiffness varies as the third power of the plate thickness while the mass has a linear relationship with the thickness. Hence, the increase in the stiffness is higher than that in the mass; therefore, upon increasing $(2h/a)$, the natural frequency would increase. Such an increase in the thickness of the piezoelectric layer affects both stiffness and mass of the plate as well as the electromechanical loading. As observed in Figure 4, increasing the thickness of the piezoelectric layer overlay decreases the natural frequency of the structure; however, the decrease in the frequency rate slows down after a specific value of piezoelectric thickness, and the curve follows an almost constant trend.

Figures 5 and 6 show the nine consecutive mode shapes of the SSSS and SCSF smart transversely isotropic plate, respectively. The value of the natural frequency of each mode is given in the bracket. In Figure 6, the mode shapes and natural frequencies of the SCSF plate are compared with those in Ref. [59], and the results are well matched.

Example 3. A square FG plate made of 'Al/Al_2O_3' with two piezoelectric (PZT-4) layers attached to the faces was studied. Tables 4–9 present the first three non-dimensional natural frequencies of the above-

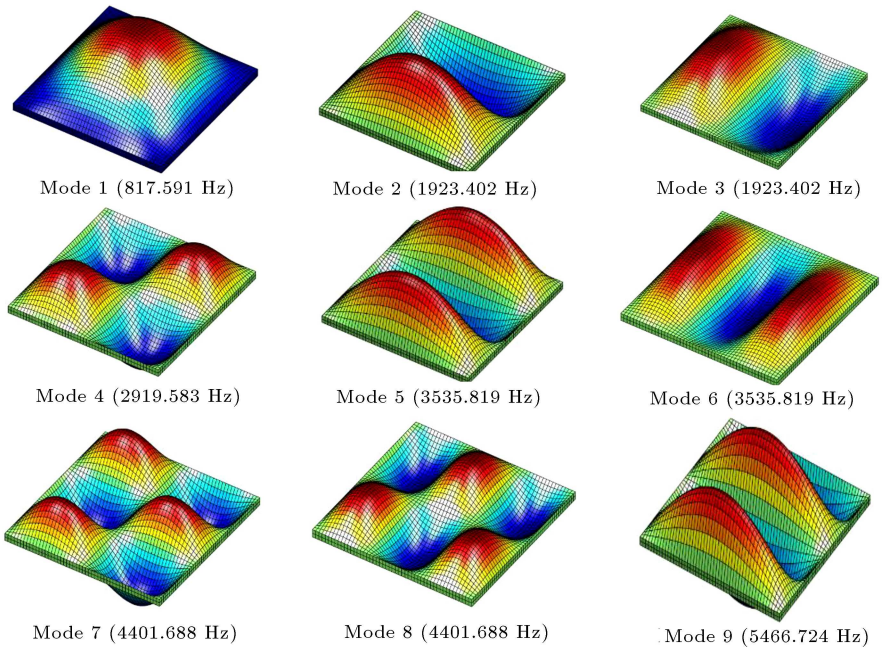

Figure 5. Nine consecutive mode shapes of SSSS smart plate.

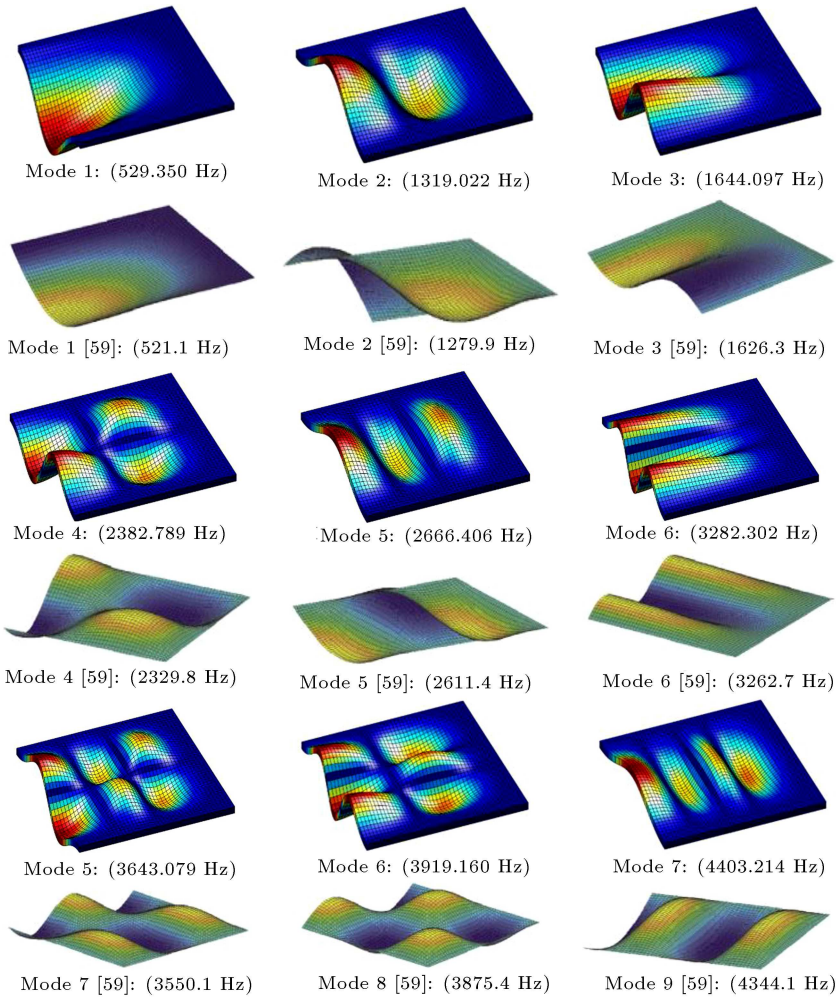

Figure 6. Nine consecutive mode shapes of SFSC smart plate compared with spectral element method results based on First-order Shear Deformation Theory (FSDT) [59].

Table 4. Natural frequencies (Hz) of the SSSS smart Functionally Graded (FG) plate.

Power-law index (n)	$\frac{2h}{a}$	$\frac{h_p}{2h}$	Method	Mode number		
				(1,1)	(1,2)	(2,2)
0	0.05	0.1	Present	426.817 [0.03]	1050.245 [0.08]	1655.019 [0.12]
			RPT [35]	426.818 [0.04]	1050.253 [0.08]	1655.040 [0.13]
			FSDT [31]	426.662	1049.356	1652.929
		0.2	Present	408.824 [0.08]	1003.121 [0.19]	1576.686 [0.29]
			RPT [35]	408.836 [0.09]	1003.195 [0.21]	1576.867 [0.31]
			FSDT [31]	408.475	1001.133	1572.036
	0.1	0.1	Present	827.509 [0.12]	1957.338 [0.24]	2983.744 [0.31]
			RPT [35]	827.520 [0.13]	1957.398 [0.25]	2983.884 [0.32]
			FSDT [31]	826.463	1952.530	2974.440
		0.2	Present	788.343 [0.29]	1849.117 [0.57]	2801.184 [0.74]
			RPT [35]	788.433 [0.31]	1849.607 [0.60]	2802.300 [0.78]
			FSDT [31]	786.011	1838.475	2780.541
0.5	0.05	0.1	Present	369.196 [0.04]	908.966 [0.11]	1433.133 [0.17]
			RPT [35]	369.195 [0.05]	908.939 [0.11]	1433.121 [0.17]
			FSDT [31]	369.015	907.918	1430.642
		0.2	Present	362.643 [0.10]	889.782 [0.24]	1398.517 [0.36]
			RPT [35]	362.655 [0.11]	889.866 [0.25]	1398.681 [0.37]
			FSDT [31]	362.269	887.637	1393.475
	0.1	0.1	Present	716.566 [0.17]	1697.962 [0.35]	2592.126 [0.46]
			RPT [35]	716.563 [0.17]	1697.781 [0.34]	2592.067 [0.46]
			FSDT [31]	715.319	1691.992	2580.078
		0.2	Present	699.259 [0.36]	1640.202 [0.72]	2484.989 [0.95]
			RPT [35]	699.343 [0.37]	1640.759 [0.76]	2486.009 [0.99]
			FSDT [31]	696.730	1628.388	2461.527

Table 4. Natural frequencies (Hz) of the SSSS smart Functionally Graded (FG) plate (continued).

Power-law index (n)	$\frac{2h}{a}$	$\frac{h_p}{2h}$	Method	Mode number		
				(1,1)	(1,2)	(2,2)
1	0.05	0.1	Present	340.004 [0.04]	836.857 [0.10]	1319.101 [0.15]
			RPT [35]	340.006 [0.04]	836.868 [0.10]	1319.055 [0.15]
			FSDT [31]	339.859	836.020	1317.115
		0.2	Present	340.656 [0.10]	835.243 [0.23]	1311.964 [0.35]
			RPT [35]	340.673 [0.11]	835.240 [0.24]	1312.112 [0.37]
			FSDT [31]	340.311	833.266	1307.323
	0.1	0.1	Present	659.550 [0.15]	1561.589 [0.30]	2382.582 [0.40]
			RPT [35]	659.565 [0.15]	1561.668 [0.31]	2382.309 [0.39]
			FSDT [31]	658.555	1556.838	2373.020
		0.2	Present	655.982 [0.35]	1535.655 [0.71]	2323.376 [0.94]
			RPT [35]	656.105 [0.37]	1535.659 [0.72]	2324.299 [0.98]
			FSDT [31]	653.652	1524.747	2301.658
2	0.05	0.1	Present	317.164 [0.01]	779.475 [0.02]	1226.974 [0.02]
			RPT [35]	317.232 [0.03]	779.552 [0.03]	1227.009 [0.03]
			FSDT [31]	317.135	779.313	1226.615
		0.2	Present	324.228 [0.07]	793.341 [0.17]	1243.871 [0.25]
			RPT [35]	324.335 [0.11]	793.467 [0.19]	1244.177 [0.28]
			FSDT [31]	323.992	791.993	1240.736
	0.1	0.1	Present	613.487 [0.03]	1446.023 [0.04]	2198.798 [0.04]
			RPT [35]	613.982 [0.11]	1446.529 [0.08]	2199.028 [0.05]
			FSDT [31]	613.305	1445.353	2197.887
		0.2	Present	621.935 [0.25]	1447.583 [0.50]	2181.080 [0.65]
			RPT [35]	622.698 [0.38]	1448.398 [0.56]	2182.913 [0.74]
			FSDT [31]	620.355	1440.316	2166.899

Table 5. Natural frequencies (Hz) of the SCSC smart Functionally Graded (FG) plate.

Power-law index (n)	$\frac{2h}{a}$	$\frac{h_p}{2h}$	Method	Mode number		
				(1,1)	(1,2)	(2,2)
0	0.05	0.1	Present	620.762 [0.70]	1160.326 [0.64]	1451.051 [1.02]
			FSDT [31]	616.446	1152.942	1436.325
		0.2	Present	594.149 [0.88]	1107.864 [0.84]	1384.012 [1.34]
			FSDT [31]	588.944	1098.612	1365.634
	0.1	0.1	Present	1177.584 [2.36]	2142.240 [1.82]	2606.281 [3.18]
			FSDT [31]	1150.432	2103.790	2525.933
		0.2	Present	1119.519 [2.93]	2022.358 [2.36]	2412.848 [2.23]
			FSDT [31]	1087.556	1975.729	2360.037
0.5	0.05	0.1	Present	537.273 [0.69]	1004.511 [0.65]	1257.258 [1.03]
			FSDT [31]	533.568	998.005	1244.321
		0.2	Present	527.137 [0.92]	982.777 [0.89]	1228.102 [1.42]
			FSDT [31]	522.330	974.076	1210.840
	0.1	0.1	Present	1021.795 [2.36]	1859.970 [1.90]	2268.644 [3.26]
			FSDT [31]	998.185	1825.231	2196.822
		0.2	Present	993.756 [3.07]	1794.477 [2.53]	2146.517 [2.66]
			FSDT [31]	964.112	1750.085	2090.820
1	0.05	0.1	Present	494.775 [0.67]	924.805 [0.63]	1157.447 [1.00]
			FSDT [31]	491.442	919.009	1145.901
		0.2	Present	495.003 [0.93]	922.389 [0.90]	1152.086 [1.44]
			FSDT [31]	490.400	914.115	1135.644
	0.1	0.1	Present	940.445 [2.31]	1710.592 [1.84]	2086.556 [3.18]
			FSDT [31]	919.203	1679.663	2022.220
		0.2	Present	931.263 [3.12]	1679.438 [2.55]	1986.789 [1.70]
			FSDT [31]	903.034	1637.542	1953.479
2	0.05	0.1	Present	461.117 [0.64]	861.029 [0.56]	1076.241 [0.91]
			FSDT [31]	458.149	856.189	1066.500
		0.2	Present	470.494 [0.95]	875.575 [0.87]	1091.568 [1.42]
			FSDT [31]	466.052	867.939	1076.265
	0.1	0.1	Present	872.172 [2.18]	1582.126 [1.59]	1923.382 [2.86]
			FSDT [31]	853.554	1557.277	1869.767
		0.2	Present	879.162 [3.12]	1580.501 [2.40]	1910.371 [3.01]
			FSDT [31]	852.529	1543.328	1854.401

Table 6. Natural frequencies (Hz) of the SSSC smart Functionally Graded (FG) plate.

Power-law index (n)	$\frac{2h}{a}$	$\frac{h_p}{2h}$	Method	Mode number		
				(1,1)	(1,2)	(2,2)
0	0.05	0.1	Present	509.680 [0.34]	1097.909 [0.30]	1238.412 [0.50]
			FSDT [31]	507.936	1094.565	1232.191
		0.2	Present	488.040 [0.45]	1048.476 [0.45]	1182.031 [0.71]
			FSDT [31]	485.851	1043.735	1173.657
	0.1	0.1	Present	979.890 [1.18]	2038.183 [0.88]	2267.081 [1.58]
			FSDT [31]	968.399	2020.226	2231.715
		0.2	Present	932.644 [1.53]	1924.835 [1.30]	2138.813 [2.17]
			FSDT [31]	918.518	1900.109	2093.283
0.5	0.05	0.1	Present	440.965 [0.34]	950.320 [0.32]	1072.377 [0.52]
			FSDT [31]	439.446	947.209	1066.737
		0.2	Present	432.939 [0.47]	930.043 [0.50]	1048.657 [0.77]
			FSDT [31]	430.892	925.412	1040.607
	0.1	0.1	Present	849.157 [1.20]	1768.702 [0.98]	1969.885 [1.68]
			FSDT [31]	839.040	1751.518	1937.295
		0.2	Present	827.467 [1.62]	1707.585 [1.45]	1898.392 [2.37]
			FSDT [31]	814.202	1683.037	1854.262
1	0.05	0.1	Present	406.091 [0.33]	874.921 [0.31]	987.271 [0.50]
			FSDT [31]	404.735	872.211	982.304
		0.2	Present	406.635 [0.48]	872.977 [0.50]	984.077 [0.78]
			FSDT [31]	404.681	868.614	976.451
	0.1	0.1	Present	781.561 [1.16]	1626.639 [0.92]	1811.684 [1.61]
			FSDT [31]	772.528	1611.695	1782.902
		0.2	Present	775.927 [1.65]	1598.479 [1.46]	1776.070 [2.40]
			FSDT [31]	763.316	1575.457	1734.388
2	0.05	0.1	Present	378.682 [0.30]	814.789 [0.23]	918.833 [0.41]
			FSDT [31]	377.523	812.863	915.005
		0.2	Present	386.829 [0.47]	828.975 [0.45]	933.609 [0.73]
			FSDT [31]	384.988	825.245	926.827
	0.1	0.1	Present	726.143 [1.05]	1505.524 [0.67]	1673.865 [1.32]
			FSDT [31]	718.539	1495.435	1651.948
		0.2	Present	734.444 [1.61]	1505.783 [1.27]	1668.991 [2.22]
			FSDT [31]	722.778	1486.802	1632.616

Table 7. Natural frequencies (Hz) of the SFSF smart Functionally Graded (FG) plate.

Power-law index (n)	$\frac{2h}{a}$	$\frac{h_p}{2h}$	Method	Mode number		
				(1,1)	(1,2)	(2,2)
0	0.05	0.1	Present	209.492 [0.17]	349.883 [1.14]	787.104 [1.38]
			FSDT [31]	209.131	345.912	776.347
		0.2	Present	200.922 [0.21]	335.361 [1.26]	751.990 [1.54]
			FSDT [31]	200.497	331.173	740.546
	0.1	0.1	Present	412.489 [0.37]	682.351 [2.31]	1490.501 [2.70]
			FSDT [31]	410.965	666.942	1451.175
		0.2	Present	394.481 [0.48]	650.523 [2.59]	1407.090 [3.09]
			FSDT [31]	392.558	634.074	1364.877
0.5	0.05	0.1	Present	181.197 [0.17]	302.686 [1.12]	680.878 [1.36]
			FSDT [31]	180.881	299.312	671.687
		0.2	Present	178.264 [0.22]	297.596 [1.27]	666.981 [1.57]
			FSDT [31]	177.869	293.841	656.662
	0.1	0.1	Present	356.968 [0.38]	590.614 [2.28]	1290.139 [2.71]
			FSDT [31]	355.590	577.414	1256.026
		0.2	Present	349.988 [0.52]	577.101 [2.64]	1246.895 [3.18]
			FSDT [31]	348.152	562.234	1208.408
1	0.05	0.1	Present	166.905 [0.17]	278.822 [1.11]	626.906 [1.35]
			FSDT [31]	166.619	275.737	618.508
		0.2	Present	167.526 [0.22]	279.673 [1.29]	626.359 [1.59]
			FSDT [31]	167.147	276.086	616.527
	0.1	0.1	Present	328.717 [0.37]	543.725 [2.26]	1186.202 [2.68]
			FSDT [31]	327.486	531.672	1155.139
		0.2	Present	328.676 [0.53]	541.727 [2.68]	1168.256 [3.22]
			FSDT [31]	326.934	527.566	1131.725
2	0.05	0.1	Present	155.799 [0.16]	260.236 [1.13]	584.469 [1.35]
			FSDT [31]	155.547	257.314	576.634
		0.2	Present	159.596 [0.22]	266.389 [1.34]	595.775 [1.63]
			FSDT [31]	159.237	262.842	586.195
	0.1	0.1	Present	306.392 [0.32]	506.354 [2.25]	1101.129 [2.62]
			FSDT [31]	305.394	495.169	1072.979
		0.2	Present	312.493 [0.50]	514.515 [2.74]	1105.406 [3.24]
			FSDT [31]	310.924	500.768	1070.684

Table 8. Natural frequencies (Hz) of the SSSF smart Functionally Graded (FG) plate.

Power-law index (n)	$\frac{2h}{a}$	$\frac{h_p}{2h}$	Method	Mode number		
				(1,1)	(1,2)	(2,2)
0	0.05	0.1	Present	253.893 [0.37]	597.759 [0.79]	880.804 [0.33]
			FSDT [31]	252.947	593.029	877.903
		0.2	Present	243.463 [0.43]	571.973 [0.91]	842.037 [0.44]
			FSDT [31]	242.419	566.812	838.279
	0.1	0.1	Present	498.358 [0.77]	1146.013 [1.60]	1658.715 [0.71]
			FSDT [31]	494.517	1127.902	1646.927
		0.2	Present	476.193 [0.93]	1087.444 [1.90]	1570.244 [1.05]
			FSDT [31]	471.776	1067.098	1553.911
0.5	0.05	0.1	Present	219.616 [0.37]	517.113 [0.79]	762.250 [0.34]
			FSDT [31]	218.802	513.044	759.598
		0.2	Present	216.018 [0.44]	507.385 [0.93]	746.999 [0.48]
			FSDT [31]	215.068	502.694	743.390
	0.1	0.1	Present	431.332 [0.78]	992.348 [1.62]	1438.222 [0.79]
			FSDT [31]	427.966	976.439	1426.860
		0.2	Present	422.483 [0.97]	964.264 [1.98]	1392.937 [1.17]
			FSDT [31]	418.392	945.459	1376.707
1	0.05	0.1	Present	202.295 [0.36]	476.200 [0.78]	701.879 [0.33]
			FSDT [31]	201.555	472.495	699.527
		0.2	Present	203.003 [0.44]	476.579 [0.94]	701.421 [0.48]
			FSDT [31]	202.095	472.115	698.014
	0.1	0.1	Present	397.169 [0.77]	912.993 [1.60]	1323.019 [0.75]
			FSDT [31]	394.126	898.589	1313.092
		0.2	Present	396.695 [0.98]	904.080 [2.01]	1304.938 [1.18]
			FSDT [31]	392.810	886.259	1289.712
2	0.05	0.1	Present	188.822 [0.36]	444.107 [0.77]	654.086 [0.27]
			FSDT [31]	188.142	440.713	652.260
		0.2	Present	193.375 [0.45]	453.467 [0.95]	666.707 [0.45]
			FSDT [31]	192.497	449.172	663.718
	0.1	0.1	Present	370.071 [0.72]	848.383 [1.51]	1226.672 [0.55]
			FSDT [31]	367.407	835.753	1219.942
		0.2	Present	376.997 [0.97]	856.245 [1.97]	1232.182 [1.02]
			FSDT [31]	373.363	839.662	1219.643

Table 9. Natural frequencies (Hz) of the SFSC smart Functionally Graded (FG) plate.

Power-law index (n)	$\frac{2h}{a}$	$\frac{h_p}{2h}$	Method	Mode number		
				(1,1)	(1,2)	(2,2)
0	0.05	0.1	Present	275.486 [0.60]	708.972 [1.16]	891.314 [0.42]
			FSDT [31]	273.825	700.789	887.562
		0.2	Present	264.155 [0.69]	677.982 [1.34]	852.062 [0.55]
			FSDT [31]	262.343	668.959	847.386
	0.1	0.1	Present	539.564 [1.39]	1344.310 [2.82]	1677.080 [0.94]
			FSDT [31]	532.143	1307.322	1661.425
		0.2	Present	515.401 [1.62]	1273.542 [3.33]	1587.470 [1.30]
			FSDT [31]	507.137	1232.470	1567.069
0.5	0.05	0.1	Present	238.311 [0.59]	613.455 [1.15]	771.367 [0.43]
			FSDT [31]	236.898	606.470	767.999
		0.2	Present	234.391 [0.70]	601.439 [1.37]	755.907 [0.58]
			FSDT [31]	232.753	593.255	751.474
	0.1	0.1	Present	467.082 [1.38]	1164.968 [2.82]	1454.244 [1.01]
			FSDT [31]	460.698	1132.986	1439.591
		0.2	Present	457.305 [1.67]	1129.490 [3.44]	1408.263 [1.43]
			FSDT [31]	449.761	1091.882	1388.371
1	0.05	0.1	Present	219.519 [0.59]	564.887 [1.13]	710.277 [0.42]
			FSDT [31]	218.230	558.530	707.271
		0.2	Present	220.268 [0.71]	564.807 [1.40]	709.784 [0.59]
			FSDT [31]	218.700	556.991	705.586
	0.1	0.1	Present	430.084 [1.36]	1071.660 [2.78]	1337.756 [0.97]
			FSDT [31]	424.284	1042.656	1324.821
		0.2	Present	429.354 [1.70]	1058.382 [3.49]	1319.261 [1.43]
			FSDT [31]	422.158	1022.599	1300.541
2	0.05	0.1	Present	204.888 [0.59]	526.575 [1.12]	661.895 [0.37]
			FSDT [31]	203.681	520.694	659.443
		0.2	Present	209.804 [0.74]	537.065 [1.44]	674.632 [0.56]
			FSDT [31]	208.259	529.439	670.847
	0.1	0.1	Present	400.635 [1.33]	994.400 [2.70]	1240.222 [0.77]
			FSDT [31]	395.346	968.255	1230.661
		0.2	Present	407.881 [1.73]	1000.418 [3.53]	1245.555 [1.29]
			FSDT [31]	400.942	966.283	1229.592

mentioned plate under different boundary conditions. In addition, the accuracies of the proposed approach and the used plate theory were evaluated by comparing the results with the FSDT-Levy solution reported by Askari Farsangi and Saidi [31] and the RPT-Navier solution reported by Rouzegar and Abad [35].

As observed, the results were in excellent agreement, indicating the accuracy of the solution method and proper performance of the iterative algorithm. Table 4 corresponds to the fully and simply supported plates where the Navier solution is applicable under this type of boundary condition. The current results and Navier solution based on the four-variable RPT [35] were compared with a Levy solution based on the FSDT [31]. The current results and those reported in [35] are very close to each other and they exhibit a negligible error in comparison to the FSDT-Levy solution [31]. The Navier method is not applicable in other types of boundary conditions. Tables 5–9 compare the obtained results with only the FSDT-Levy solution [31], and the percentage errors for all cases are in acceptable ranges. The number of iterations required to achieve a converged result for the mode (1,1) of the smart FG plate ($n = 0.5$, $2h/a = 0.05$, $h_p/2h = 0.1$) is 375, 545, 447, 246, 225, and 188 cycles for the SSSS, SCSC, SSSC, SFSC, SSSF, and SFSF plates, respectively.

Figure 7 shows the variation in the fundamental frequency of fully and simply supported smart FG plates versus the piezoelectric thickness for several power-law indices. To better understand the impact of the piezoelectric layer on the vibrational behavior of the FG plate, parameter β is defined by Eq. (64) as shown in Box VI. Figure 8 illustrates the variations in parameter β against the piezoelectric thickness for several power-law indices. Addition of the piezoelectric layer can affect the frequency of the plate in three ways: increasing the structural stiffness, increasing the mass, and creating a load related to electromechanical coupling in the piezoelectric layer. An increase in the structural stiffness increases the natural frequency. On the contrary, an increase in mass decreases the natural frequency. Further, the induced electromechanical loading has a significant effect on natural frequency. Therefore, adding the piezoelectric layer may finally lead to either increase or decrease in the natural frequency.

Depending on the value of the power index that

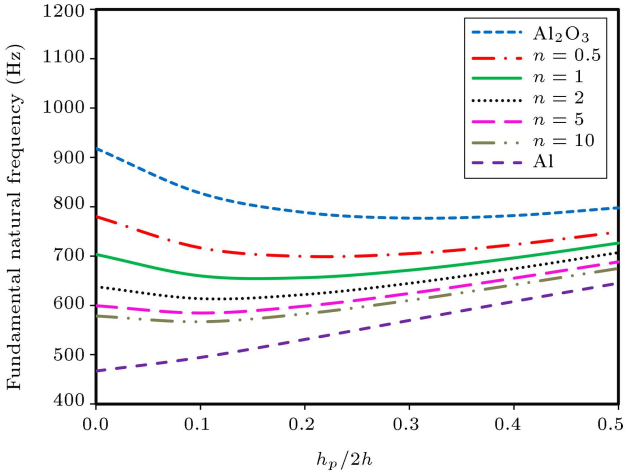

Figure 7. Fundamental frequency of the SSSS smart Functionally Graded (FG) plate versus the piezoelectric layer thickness considering different power-law index values ($2h/a = 0.1$).

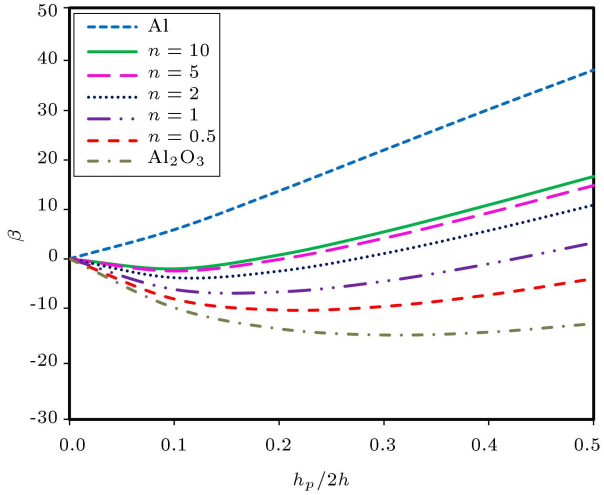

Figure 8. Parameter β of the SSSS smart Functionally Graded (FG) plate versus piezoelectric layer thickness considering different power-law index values ($2h/a = 0.1$).

influences the stiffness and mass of the FG core plate, the effect of the piezoelectric layer on the natural frequency and parameter varies. As seen in Figure 7, for low power-law indices, increasing the thickness of the piezoelectric layer causes a decrease in the natural frequency in the first part of the diagram and then, induces an increase in it. As a result, parameter β is initially negative and then, it tends to become positive, followed by increasing the thickness

$$\beta = \frac{\omega_{\text{structure with piezoelectric layer}} - \omega_{\text{structure without piezoelectric layer}}}{\omega_{\text{structure without piezoelectric layer}}} \times 100. \tag{64}$$

Box VI

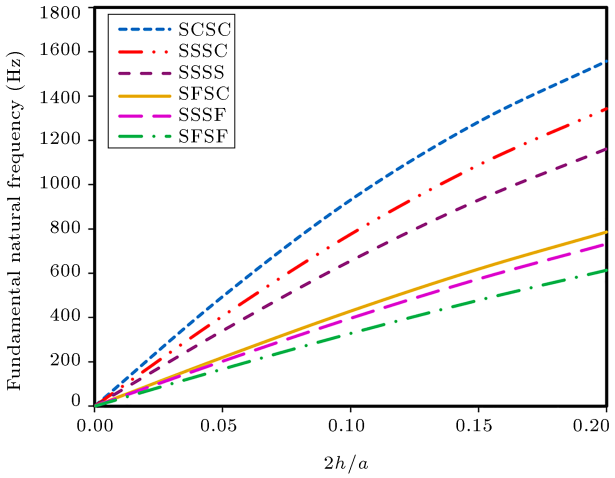

Figure 9. Fundamental frequency (ω) of the smart Functionally Graded (FG) plate versus the thickness-to-side ratio considering different Levy-type boundary conditions ($n = 1$ and $h_p/2h = 0.2$).

of the piezoelectric layer. For higher power-law indices, increasing the value $h_p/2h$ leads to an increase in the natural frequency with a steeper slope. To be specific, upon increasing the mentioned thickness, when the core plate is pure 'Al', the natural frequency always follows an ascending trend; therefore, parameter β is always positive. According to Figure 7, for a specific value of piezoelectric layer thickness, while increasing the power-law index (moving from pure 'Al_2O_3' to pure 'Al'), the frequency of the smart FG plate decreases due to the lower value of elastic modulus of 'Al' than that of 'Al_2O_3'. According to Figures 7 and 8, there is an optimum value for the piezoelectric layer thickness that results in a minimum natural frequency, which can be used for designing smart FG plates and determining proper piezoelectric thickness. Finally, the effect of Levy-type boundary conditions on the variations in the fundamental natural frequency of the smart FG plate (with $n = 1$ and $h_p/2h = 0.2$) versus the $2h/a$ is investigated in Figure 9. For all types of boundary conditions, increasing the thickness-to-side ratio intensifies the plate stiffness and consequently, increases the natural frequency. The slope of the curves depends on the type of boundary condition where the curve related to the SFSF boundary condition with the lowest constraint possesses the lowest slope and the SCSC has the highest slope. As expected, at a specific value of the thickness-to-side ratio, natural frequency follows an upward trend by moving from the SFSF boundary condition with the lowest constraint to the SCSC case with the highest constraint.

4. Conclusion

The present study investigated the problem of free vibration of an Functionally Graded (FG) core plate with a pair of piezoelectric layers attached to its top and bottom surfaces. To this end, a simple yet efficient four-variable refined plate theory was utilized that yielded accurate results for both thin and thick plates. Two opposite edges of the pale were simply supported and two other edges were exposed to arbitrary boundary conditions. The state-space approach and Levy solution were employed to solve the governing equations. To the best of the authors' knowledge, this is the first time that this approach is proposed for free vibration analysis of the mentioned smart FG plates in different Levy-type boundary conditions. An assessment of the obtained results and their counterparts in the literature revealed that the proposed theory and its corresponding solution exhibited acceptable accuracy. This study also evaluated the effects of different parameters, the results of which are summarized below:

- With an increase in the thickness-to-side ratio, the plate thickness and consequently the mass and stiffness of the structure increased. Of note, the increase in the stiffness was more intensive than that in the mass, hence an increase in the natural frequency;
- Adding the piezoelectric layer to the main structure or changing its thickness had considerable effects on the stiffness and mass of the structure as well as the induced loading due to electromechanical coupling. Depending on the value of each of the three above-mentioned factors, the thicker piezoelectric layer might result in an increase or decrease in the natural frequency;
- For the given power-law index, an optimum value of the piezoelectric layer thickness was found wherein the natural frequency of the smart FG plate was minimum. Determining this value could help design the structure and determine the piezoelectric layer thickness;
- More constraints at the edges would result in an increase in the structural stiffness and natural frequency;
- As the aspect ratio of the plate (a/b) increased (considering a constant value for a), the natural frequency also increased due to the increase in the plate stiffness;
- Since the modulus of elasticity of 'Al' was lower than that of 'Al_2O_3', increasing the power-law index led to a reduction in the plate stiffness and structural natural frequency.

Nomenclature

A_{ij}, A^s_{11}	Stiffness coefficient matrices
B_{ij}, D_{ij}	Stiffness coefficient matrices

G_{ij}, F_{ij}, H_{ij}	Stiffness coefficient matrices
a, b	Plate length and width
$\hat{\mathbf{a}}$	Matrix defined for evaluation of the boundary conditions
$\mathbf{C}, Q$	Matrix of elastic constant for the piezoelectric layer and FG core plate
c_i, q_i	Coefficients in the transfer matrix
$\mathbf{d}$	Electric displacement vector
E	Young's modulus of elasticity
$\mathbf{e}$	Piezoelectric constant matrix
f	Distribution function of the in-plane displacements
g	Defined function in strain tensor
h, h_p	Half-thickness of the FG plate and Piezoelectric layer thickness
I_0 to I_5	Mass moment of inertia
j	Imaginary unit ($\sqrt{-1}$)
$\mathbf{K}$	Kinetic energy
$\mathbf{k}, \mathbf{P}$	Constant vectors in the state-space equation
$\mathbf{L}, \mathbf{l}$	Matrices defined in the eigenvalue equation
M, N, S	Stress resultants
$\mathbf{n}$	Power-law index
$\bar{P}_i$	Constant vector components in the eigenvalue equation
R_{ij}	Matrix components in the eigenvalue equation
$\mathbf{T}$	Transfer matrix
t	Time
U	Strain energy
U_m, V_m	Unknown parameters in Levy series expansion
W_{bm}, w_{sm}	Unknown parameters in Levy series expansion
u, v	In-plane displacements in the x and y directions
u_i, v_i	Real and imaginary part of eigenvalues
V	Volume of the plate
w	Transverse displacement
w_b, w_s	Bending and shear component of transverse displacement
$\mathbf{X}$	Eigenvector
x, y, z	Cartesian coordinates
$\mathbf{Z}$	State vector
$\boldsymbol{\alpha}$	The angle of the sinus and cosine in Levy solution
β	Non-dimensional parameter
γ	Shear strain
$\delta, \psi, \lambda, \hbar, \chi$	Coefficients in transfer matrix
ε	Normal strain
$\boldsymbol{\eta}$	Dielectric constant matrix
λ_i	Eigenvalues
μ_i	Parameters defined in the weak form of the governing equation
ξ_i	Parameters defined in Maxwell's equation
ρ	Mass density
$\boldsymbol{\sigma}$	Stress
υ	Poisson's ratio
φ	Parameter defined in the electrostatic potential equation
φ_m	Unknown parameter in Levy series expansion
ω_m	Natural frequency
$\bar{\omega}$	Non-dimensional frequency
$\boldsymbol{\Xi}$	Electric field intensity vector
ϕ	Electrostatic potential
ℓ_i and ℓ_{ij}	Coefficients in the free boundary condition

References

1. Nguyen-Thanh, N., Li, W., and Zhou, K. "Static and free-vibration analyses of cracks in thin-shell structures based on an isogeometric-meshfree coupling approach", *Comput. Mech.*, **62**, pp. 1287–1309 (2018).
2. Tan, P., Nguyen-Thanh, N., Rabczuk, T., et al. "Static, dynamic and buckling analyses of 3D FGM plates and shells via an isogeometric-meshfree coupling approach", *Compos. Struct.*, **15**, pp. 35–50 (2018).
3. Li, Y., Xiong, F., Xie, L., et al. "State-space approach for transverse vibration of double-beam systems", *Int. J. Mech. Sci.*, **189**, p. 105974 (2021).
4. Abrate, S. "Functionally graded plates behave like homogeneous plates", *Compos. Part B-Eng.*, **39**, pp. 151–158 (2008).
5. Yin, S., Yu, T., and Liu, P. "Free vibration analyses of FGM thin plates by isogeometric analysis based on classical plate theory and physical neutral surface", *Adv. Mech. Eng.*, **5**, 634584 (2013).
6. Huang, J., Nguyen-Thanh, N., and Zhou, K. "Extended isogeometric analysis based on Bézier extraction for the buckling analysis of Mindlin-Reissner plates", *Acta Mech.*, **228**, pp. 3077–3093 (2017).
7. Hosseini-Hashemi, S., Taher, H.R.D., Akhavan, H., et al. "Free vibration of functionally graded rectangular plates using first-order shear deformation plate theory", *Appl. Math. Model.*, **34**, pp. 1276–1291 (2010).
8. Thai, H.T. and Choi, D.H. "A simple first-order shear deformation theory for the bending and free vibration analysis of functionally graded plates", *Compos. Struct.*, **101**, pp. 332–340 (2013).

9. Thai, H.T., Nguyen, T.K., Vo, T.P., et al. "Analysis of functionally graded sandwich plates using a new first-order shear deformation theory", *Eur. J. Mech. A-Solids*, **45**, pp. 211–225 (2014).

10. Anamagh, M.R. and Bediz, B. "Free vibration and buckling behavior of functionally graded porous plates reinforced by graphene platelets using spectral Chebyshev approach", *Compos. Struct.*, **253**, p. 112765 (2020).

11. Matsunaga, H. "Free vibration and stability of functionally graded plates according to a 2-D higher-order deformation theory", *Compos. Struct.*, **82**, pp. 499–512 (2008).

12. Baferani, A.H., Saidi, A.R., and Ehteshami, H. "Accurate solution for free vibration analysis of functionally graded thick rectangular plates resting on elastic foundation", *Compos. Struct.*, **93**, pp. 1842–1853 (2011).

13. Ebrahimi, F. and Heidari, E. "Surface effects on nonlinear vibration of embedded functionally graded nanoplates via higher order shear deformation plate theory", *Mech. Adv. Mater. Struc.*, **26**, pp. 671–699 (2019).

14. Belkhodja, Y., Ouinas, D., Zaoui, F.Z., et al. "An exponential-trigonometric higher order shear deformation theory (HSDT) for bending, free vibration, and buckling analysis of functionally graded materials (FGMs) plates", *Adv. Compos. Lett.*, **29**, 0963693519875739 (2020).

15. Shimpi, R.P. "Refined plate theory and its variants", *AIAA J.*, **40**, pp. 137–146 (2002).

16. Benachour, A., Tahar, H.D., Atmane, H.A., et al. "A four variable refined plate theory for free vibrations of functionally graded plates with arbitrary gradient", *Compos. Part B-Eng.*, **42**, pp. 1386–1394 (2011).

17. Thai, H.T. and Choi, D.H. "A refined shear deformation theory for free vibration of functionally graded plates on elastic foundation", *Compos. Part B-Eng.*, **43**, pp. 2335–2347 (2012).

18. Hadji, L., Atmane, H.A., Tounsi, A., et al. "Free vibration of functionally graded sandwich plates using four-variable refined plate theory", *Appl. Math. Mech.*, **32**, pp. 925–942 (2011).

19. Mechab, I., Mechab, B., and Benaissa, S. "Static and dynamic analysis of functionally graded plates using four-variable refined plate theory by the new function", *Compos. Part B-Eng.*, **45**, pp. 748–757 (2013).

20. Demirhan, P.A. and Taskin, V. "Bending and free vibration analysis of Levy-type porous functionally graded plate using state space approach", *Compos. Part B-Eng.*, **160**, pp. 661–676 (2019).

21. Tan, P., Nguyen-Thanh, N., and Zhou, K. "Extended isogeometric analysis based on Bézier extraction for an FGM plate by using the two-variable refined plate theory", *Theor. Appl. Fract. Mech.*, **89**, pp. 127–38 (2017).

22. Le, C.I., Pham, V.N., and Nguyen, D.K. "Free vibration of FGSW plates partially supported by pasternak foundation based on refined shear deformation theories", *Math. Probl. Eng.* (2020). https://doi.org/10.1155/2020/7180453

23. Abrate, S. and Di Sciuva, M. "Equivalent single layer theories for composite and sandwich structures: A review", *Compos. Struct.*, **179**, pp. 482–494 (2017).

24. Iurlaro, L., Gherlone, M., and Di Sciuva, M. "Bending and free vibration analysis of functionally graded sandwich plates using the refined zigzag theory", *J. Sandw. Struct. Mater.*, **16**, pp. 669–699 (2014).

25. Ghorbanpour Arani, A., Mosayyebi, M., Kolahdouzan, F., et al. "Refined zigzag theory for vibration analysis of viscoelastic functionally graded carbon nanotube reinforced composite microplates integrated with piezoelectric layers", *Proceedings of the Institution of Mechanical Engineers, Part G: J. Aerosp. Eng.*, **231**, pp. 2464–2478 (2017).

26. Abrate, S. and Di Sciuva, M. "Multilayer models for composite and sandwich structures", *Comprehensive Composite Materials II*, P.W.R. Beaumont, and C.H. Zweben, Eds., Elsevier, pp. 399–425 (2018).

27. Di Sciuva, M. and Sorrenti, M. "Bending and free vibration analysis of functionally graded sandwich plates: An assessment of the refined zigzag theory", *J. Sandw. Struct. Mater.*, **23**, pp. 1–43 (2019).

28. Di Sciuva, M. and Sorrenti, M. "Bending, free vibration and buckling of functionally graded carbon nanotube-reinforced sandwich plates, using the extended refined zigzag theory", *Compos. Struct.*, **227**, p. 111324 (2019).

29. Dorduncu, M. "Stress analysis of sandwich plates with functionally graded cores using peridynamic differential operator and refined zigzag theory", *Thin-Walled Struct.*, **146**, p. 106468 (2020).

30. He, X.Q., Ng, T.Y., Sivashanker, S., et al. "Active control of FGM plates with integrated piezoelectric sensors and actuators", *Int. J. Solids Struct.*, **38**, pp. 1641–1655 (2001).

31. Askari Farsangi, M. and Saidi, A.R. "Levy type solution for free vibration analysis of functionally graded rectangular plates with piezoelectric layers", *Smart Mater. Struct.*, **21**, p. 094017 (2012).

32. Askari Farsangi, M., Saidi, A.R., and Batra, R.C. "Analytical solution for free vibrations of moderately thick hybrid piezoelectric laminated plates", *J. Sound Vib.*, **332**, pp. 5981–5998 (2013).

33. Alibeigloo, A. "Free vibration analysis of functionally graded carbon nanotube-reinforced composite cylindrical panel embedded in piezoelectric layers by using theory of elasticity", *Eur. J. Mech. A-Solids.*, **44**, pp. 104–115 (2014).

34. Bruant, I. and Proslier, L. "Improved active control of a functionally graded material beam with piezoelectric patches", *J. Vib. Control.*, **21**, pp. 2059–80 (2015).

35. Rouzegar, J. and Abad, F. "Free vibration analysis of FG plate with piezoelectric layers using four-variable refined plate theory", *Thin-Walled Struct.*, **89**, pp. 76–83 (2015).

36. Abad, F. and Rouzegar, J. "An exact spectral element method for free vibration analysis of FG plate integrated with piezoelectric layers", *Compos. Struct.*, **180**, pp. 696–708 (2017).

37. El Harti, K., Rahmoune, M., Sanbi, M., et al. "Finite element model of vibration control for an exponential functionally graded Timoshenko beam with distributed piezoelectric sensor/actuator", *Actuators.*, **8**, p. 19 (2019).

38. Zhang, S.Q., Gao, Y.S., Zhao, G.Z., et al. "Geometrically nonlinear analysis of CNT-reinforced functionally graded composite plates integrated with piezoelectric layers", *Compos. Struct.*, **234**, p. 111694 (2020).

39. Shahdadi, A. and Rahnama, H. "Free vibration of a functionally graded annular sector plate integrated with piezoelectric layers", *Appl. Math. Model.*, **79**, pp. 341–361 (2020).

40. Rouzegar, J. and Davoudi, M. "Forced vibration of smart laminated viscoelastic plates by RPT finite element approach", *Acta Mech. Sinica*, **36**, pp. 933–949 (2020).

41. Aghakhani, A., Motlagh, P.L., Bediz, B., et al. "A general electromechanical model for plates with integrated piezo-patches using spectral-Tchebychev method", *J. Sound. Vib.*, **458**, pp. 74–88 (2019).

42. Motlagh, P.L., Anamagh, M.R., Bediz, B., et al. "Electromechanical analysis of functionally graded panels with surface-integrated piezo-patches for optimal energy harvesting", *Compos. Struct.*, **263**, p. 113714 (2021).

43. Chen, W.Q. and Ding, H.J. "On free vibration of a functionally graded piezoelectric rectangular plate", *Acta Mech.*, **153**, pp. 207–216 (2002).

44. Kapuria, S. and Achary, G.G.S. "Exact 3D piezoelasticity solution of hybrid cross-ply plates with damping under harmonic electro-mechanical loads", *J. Sound Vib.*, **282**, pp. 617–634 (2005).

45. Bian, Z.G., Ying, J., Chen, W.Q., et al. "Bending and free vibration analysis of a smart functionally graded plate", *Struct. Eng. Mech.*, **23**, pp. 97–113 (2006).

46. Yas, M.H., Jodaei, A., Irandoust, S., et al. "Three-dimensional free vibration analysis of functionally graded piezoelectric annular plates on elastic foundations", *Meccanica*, **47**, pp. 1401–1423 (2012).

47. Jodaei, A., Jalal, M., and Yas, M.H. "Three-dimensional free vibration analysis of functionally graded piezoelectric annular plates via SSDQM and comparative modeling by ANN", *Math. Comput. Modell.*, **57**, pp. 1408–1425 (2013).

48. Yas, M.H. and Moloudi, N. "Three-dimensional free vibration analysis of multi-directional functionally graded piezoelectric annular plates on elastic foundations via state space based differential quadrature method", *Appl. Math. Mech.*, **36**, pp. 439–464 (2015).

49. Xin, L. and Hu, Z. "Free vibration of simply supported and multilayered magneto-electro-elastic plates", *Compos. Struct.*, **121**, pp. 344–350 (2015).

50. Feri, M., Alibeigloo, A., and Zanoosi, A.P. "Three dimensional static and free vibration analysis of cross-ply laminated plate bonded with piezoelectric layers using differential quadrature method", *Meccanica*, **51**, pp. 921–937 (2016).

51. Ezzin, H., Amor, M.B., and Ghozlen, M.H. "Lamb waves propagation in layered piezoelectric/piezomagnetic plates", *Ultrasonics*, **76**, pp. 63–69 (2017).

52. Safarpour, M., Rahimi, A.R., and Alibeigloo, A. "Static and free vibration analysis of graphene platelets reinforced composite truncated conical shell, cylindrical shell, and annular plate using theory of elasticity and DQM", *Mech. Based Des. Struct. Mach.*, **48**, pp. 496–524 (2020).

53. Thai, H.T. and Kim, S.E. "Analytical solution of a two variable refined plate theory for bending analysis of orthotropic Levy-type plates", *Int. J. Mech. Sci.*, **54**, pp. 269–276 (2012).

54. Tiersten, H.F., *Linear Piezoelectric Plate Vibrations: Elements of the Linear Theory of Piezoelectricity and the Vibrations Piezoelectric Plates*, Springer (2013).

55. Wang, Q., Quek, S.T., Sun, C.T., et al. "Analysis of piezoelectric coupled circular plate", *Smart Mater. Struct.*, **10**, pp. 229–239 (2001).

56. Franklin, J.N. "Matrix theory", Courier Corporation (2012).

57. Jin, G., Su, Z., Shi, S., et al. "Three-dimensional exact solution for the free vibration of arbitrarily thick functionally graded rectangular plates with general boundary conditions", *Compos. Struct.*, **108**, pp. 565–577 (2014).

58. Zaoui, F.Z., Ouinas, D., and Tounsi, A. "New 2D and quasi-3D shear deformation theories for free vibration of functionally graded plates on elastic foundations", *Compos. Part B-Eng.*, **159**, pp. 231–247 (2019).

59. Abad, F. and Rouzegar, J. "Exact wave propagation analysis of moderately thick Levy-type plate with piezoelectric layers using spectral element method", *Thin-Walled Struct.*, **141**, pp. 319–331 (2019).

Appendix A

The coefficients c_i, c_{ij}, and c_{ijm} in Eqs. (40)–(44) are expressed as:

$$c_1 = \frac{A_{11}\,\alpha^2 - I_0\omega_m^2}{A_{66}}, \tag{A.1}$$

$$c_2 = \frac{-(A_{12} + A_{66})\alpha}{A_{66}}, \tag{A.2}$$

$$c_3 = \frac{-B_{11}\alpha^3 + I_1\omega_m^2\alpha}{A_{66}}, \tag{A.3}$$

$$c_4 = \frac{(B_{12} + 2B_{66})\alpha}{A_{66}}, \tag{A.4}$$

$$c_{3s} = \frac{-D_{11}\alpha^3 + I_3\omega_m^2\alpha}{A_{66}}, \tag{A.5}$$

$$c_{4s} = \frac{(D_{12} + 2D_{66})\alpha}{A_{66}}, \tag{A.6}$$

$$c_5 = \frac{(A_{12} + A_{66})\alpha}{A_{22}}, \tag{A.7}$$

$$c_6 = \frac{(A_{66}\alpha^2 - I_0\omega_m^2)}{A_{22}}, \tag{A.8}$$

$$c_7 = \frac{-(B_{12} + 2B_{66})\alpha^2 + I_1\omega_m^2}{A_{22}}, \tag{A.9}$$

$$c_{7s} = \frac{-(D_{12} + 2D_{66})\alpha^2 + I_3\omega_m^2}{A_{22}}, \tag{A.10}$$

$$c_8 = \frac{B_{22}}{A_{22}}, \tag{A.11}$$

$$c_{8s} = \frac{D_{22}}{A_{22}}, \tag{A.12}$$

$$c_{11m} = \frac{\xi_3\alpha^2}{\xi_2}, \tag{A.13}$$

$$c_{12m} = \frac{-\xi_3}{\xi_2}, \tag{A.14}$$

$$c_{13m} = \frac{-\xi_1\alpha^2}{\xi_2}, \tag{A.15}$$

$$c_{14m} = \frac{\xi_1}{\xi_2}, \tag{A.16}$$

$$c_{15m} = \frac{(\xi_2\alpha^2 + \xi_4)}{\xi_2}, \tag{A.17}$$

$$c_{9s} = \frac{(D_{11}\alpha^3 + c_1\delta + q_1\hbar - I_3\omega_m^2\alpha)}{\lambda}, \tag{A.18}$$

$$c_{10s} = \frac{(D_{22}c_6 + c_2\delta - (D_{12} + 2D_{66})\alpha^2 + q_2\hbar + I_3\omega_m^2)}{\lambda}, \tag{A.19}$$

Eqs. (A.20)–(A.23) are shown in Box A.I.

$$c_{15s} = \frac{((c_{15m} - \alpha^2)(\mu_3 - \mu_2) + q_7\hbar)}{\lambda}, \tag{A.24}$$

$$c_9 = (q_1 + c_{9s}q_8), \tag{A.25}$$

$$c_{10} = (q_2 + c_{10s}q_8), \tag{A.26}$$

$$c_{11} = (q_3 + c_{11s}q_8), \tag{A.27}$$

$$c_{12} = (q_4 + c_{12s}q_8), \tag{A.28}$$

$$c_{13} = (q_5 + c_{13s}q_8), \tag{A.29}$$

$$c_{14} = (q_6 + c_{14s}q_8), \tag{A.30}$$

$$c_{15} = (q_7 + c_{15s}q_8), \tag{A.31}$$

where:

$$\psi = (B_{22}c_5 - (B_{12} + 2B_{66})\alpha), \tag{A.32}$$

$$\chi = G_{22} - c_8B_{22}, \tag{A.33}$$

$$q_1 = \frac{(B_{11}\alpha^3 + c_1\psi - I_1\omega_m^2\alpha)}{\chi}, \tag{A.34}$$

$$q_2 = \frac{(B_{22}c_6 + c_2\psi - (B_{12} + 2B_{66})\alpha^2 + I_1\omega_m^2)}{\chi}, \tag{A.35}$$

$$c_{11s} = \frac{(c_3\delta - F_{11}\alpha^4 + c_{11m}(\mu_3 - \mu_2) + q_3\hbar + I_0\omega_m^2 + I_4\omega_m^2\alpha^2)}{\lambda}, \tag{A.20}$$

$$c_{12s} = \frac{(D_{22}c_7 + c_4\delta + 2(F_{12} + 2F_{66})\alpha^2 + c_{12m}(\mu_3 - \mu_2) + q_4\hbar - I_4\omega_m^2)}{\lambda}, \tag{A.21}$$

$$c_{13s} = \frac{(c_{3s}\delta - H_{11}\alpha^4 - A_{11}^s\alpha^2 + c_{13m}(\mu_3 - \mu_2) + q_5\hbar + I_0\omega_m^2 + I_5\omega_m^2\alpha^2)}{\lambda}, \tag{A.22}$$

$$c_{14s} = \frac{(D_{22}c_{7s} + c_{4s}\delta + 2(H_{12} + 2H_{66})\alpha^2 + A_{11}^s + c_{14m}(\mu_3 - \mu_2) + q_6\hbar - I_5\omega_m^2)}{\lambda}. \tag{A.23}$$

Box A.I

$$q_3 = \frac{(c_3\psi - G_{11}\alpha^4 - \mu_1 c_{11m} + I_0\omega_m^2 + I_2\omega_m^2\alpha^2)}{\chi}, \tag{A.36}$$

$$q_4 = \frac{(B_{22}c_7 + c_4\psi + 2(G_{12}+2G_{66})\alpha^2 - \mu_1 c_{12m} - I_2\omega_m^2)}{\chi}, \tag{A.37}$$

$$q_5 = \frac{(c_{3s}\psi - F_{11}\alpha^4 - \mu_1 c_{13m} + I_0\omega_m^2 + I_4\omega_m^2\alpha^2)}{\chi}, \tag{A.38}$$

$$q_6 = \frac{(B_{22}c_{7s} + c_{4s}\psi + 2(F_{12}+2F_{66})\alpha^2 - \mu_1 c_{14m} - I_4\omega_m^2)}{\chi}, \tag{A.39}$$

$$q_7 = \frac{(\mu_1\alpha^2 - \mu_1 c_{15m})}{\chi}, \tag{A.40}$$

$$q_8 = \frac{(c_{8s}B_{22} - F_{22})}{\chi}, \tag{A.41}$$

$$\delta = (D_{22}\,c_5 - (D_{12}+2D_{66})\,\alpha), \tag{A.42}$$

$$\lambda = H_{22} - D_{22}\,c_{8s} - q_8(D_{22}\,c_8 - F_{22}), \tag{A.43}$$

$$\hbar = D_{22}\,c_8 - F_{22}. \tag{A.44}$$

Appendix B

The factors ℓ_i and ℓ_{ij} in Eq. (58) are expressed as:

$$\ell_1 = (B_{22}c_5 - B_{12}\alpha - 2B_{66}\alpha), \tag{B.1}$$

$$\ell_2 = (B_{22}c_6 + I_1\omega_m^2 - 2B_{66}\alpha^2), \tag{B.2}$$

$$\ell_3 = (B_{22}c_7 + G_{12}\alpha^2 - I_2\,\omega_m^2 + 4G_{66}\alpha^2), \tag{B.3}$$

$$\ell_4 = (B_{22}c_{7s} + F_{12}\alpha^2 - I_4\omega_m^2 + 4F_{66}\alpha^2), \tag{B.4}$$

$$\ell_5 = (B_{22}c_8 - G_{22}), \tag{B.5}$$

$$\ell_6 = (B_{22}c_{8s} - F_{22}), \tag{B.6}$$

$$\ell_7 = -\mu_1, \tag{B.7}$$

$$\ell_8 = (D_{22}c_5 - D_{12}\alpha - 2D_{66}\alpha), \tag{B.8}$$

$$\ell_9 = (D_{22}c_6 + I_3\omega_m^2 - 2D_{66}\alpha^2), \tag{B.9}$$

$$\ell_{10} = (D_{22}c_7 + F_{12}\alpha^2 - I_4\omega_m^2 + 4F_{66}\alpha^2), \tag{B.10}$$

$$\ell_{11} = (D_{22}c_{7s} + H_{12}\alpha^2 - I_5\omega_m^2 + A_{11}^s + 4H_{66}\alpha^2), \tag{B.11}$$

$$\ell_{12} = (D_{22}c_8 - F_{22}), \tag{B.12}$$

$$\ell_{13} = (D_{22}c_{8s} - H_{22}), \tag{B.13}$$

$$\ell_{14} = \mu_3, \tag{B.14}$$

Appendix C

For very thin plates, some of the elements of matrix **I** in Eq. (61) may become extremely large or small. As observed, followed by calculating the eigenvalues of the transfer matrix, the real part of some eigenvalues u_i in $(\lambda_i = u_i + jv_i,\ j = \sqrt{-1})$ has relatively large positive or negative values. This leads to computer underflow or overflow due to the presence of an exponential function in the coefficient matrix. The eigenvalue equation is given below:

$$[\mathbf{R}]\begin{bmatrix} e^{\lambda_1 y} & & 0 \\ & \ddots & \\ 0 & & e^{\lambda_{14} y} \end{bmatrix}\{\mathbf{P}\} = \{\mathbf{0}\}, \tag{C.1}$$

$$[\mathbf{R}] = [\hat{\mathbf{a}}]\,[\mathbf{X}]\,. \tag{C.2}$$

Eq. (C.3) is shown in Box C.I. If it is assumed that $e^{u_1 b/2}$ has a large positive value, then we continue as follows. If parameter $\bar{P}_1$ is defined as:

$$\bar{P}_1 = e^{u_1 b/2} P_1, \tag{C.4}$$

then, the following relationships will be derived:

$$R_{i1}e^{-\lambda_1 b/2}P_1 = R_{i1}(e^{-jv_1 b/2}/e^{u_1 b})\bar{P}_1 \cong 0\cdot\bar{P}_1,$$

$$i = 1, ..., 8, \tag{C.5}$$

$$R_{i1}e^{\lambda_1 b/2}P_1 = R_{i1}e^{jv_1 b/2}\bar{P}_1, \quad i = 8, ..., 14. \tag{C.6}$$

Therefore, the first column of the coefficient matrix is:

$$\Big\{0\ 0\ \cdots\ 0\ R_{81}e^{jv_1 b/2}\ R_{91}e^{jv_1 b/2}\ \cdots\ R_{141}e^{jv_1 b/2}\Big\}^T. \tag{C.7}$$

Then, replace P_1 by $\bar{P}_1$. Therefore, if $e^{u_2 b/2}$ has a large negative value, the second column of the coefficient matrix is replaced by:

$$\Big\{R_{12}e^{-jv_2 b/2}\quad R_{22}e^{-jv_2 b/2}\quad \ldots\quad R_{72}e^{-jv_2 b/2}\quad 0\quad 0\quad \ldots\quad 0\Big\}^T, \tag{C.8}$$

and P_2 is replaced by $e^{u_2 b/2}\bar{P}_2$. The same procedure should be applied to other columns of the coefficient matrix.

$$\begin{bmatrix} R_{11}e^{-\lambda_1 b/2} & R_{12}e^{-\lambda_2 b/2} & \cdots & R_{114}e^{-\lambda_{14} b/2} \\ R_{21}e^{-\lambda_1 b/2} & R_{22}e^{-\lambda_2 b/2} & \cdots & R_{214}e^{-\lambda_{14} b/2} \\ \vdots & \vdots & & \vdots \\ R_{61}e^{-\lambda_1 b/2} & R_{62}e^{-\lambda_2 b/2} & \cdots & R_{614}e^{-\lambda_{14} b/2} \\ R_{71}e^{-\lambda_1 b/2} & R_{72}e^{-\lambda_2 b/2} & \cdots & R_{714}e^{-\lambda_{14} b/2} \\ R_{81}e^{\lambda_1 b/2} & R_{82}e^{\lambda_2 b/2} & \cdots & R_{814}e^{\lambda_{14} b/2} \\ R_{91}e^{\lambda_1 b/2} & R_{92}e^{\lambda_2 b/2} & \cdots & R_{914}e^{\lambda_{14} b/2} \\ \vdots & \vdots & & \vdots \\ R_{131}e^{\lambda_1 b/2} & R_{132}e^{\lambda_2 b/2} & \cdots & R_{1314}e^{\lambda_{14} b/2} \\ R_{141}e^{\lambda_1 b/2} & R_{142}e^{\lambda_2 b/2} & \cdots & R_{1414}e^{\lambda_{14} b/2} \end{bmatrix} \begin{Bmatrix} P_1 \\ P_2 \\ \vdots \\ \\ \vdots \\ \\ \vdots \\ \\ P_{14} \end{Bmatrix} = \begin{Bmatrix} 0 \\ 0 \\ \vdots \\ \\ \vdots \\ \\ \vdots \\ \\ 0 \end{Bmatrix}. \tag{C.3}$$

Box C.I

Biographies

Jafar Rouzegar is currently an Assistant Professor at the Department of Mechanical and Aerospace Engineering of Shiraz University of Technology, Iran. He received his BSc in Mechanical Engineering from Shiraz University, Iran in 2002. He also received his MSc and PhD in Mechanical Engineering from Tarbiat Modares University, Iran in 2004 and 2010, respectively. His research interests include FEM and XFEM, theories of plates and shells, and fracture mechanics.

Niloufar Salmanpour received her BSc in Mechanical Engineering from Shiraz University, Shiraz, Iran in 2015. She also received her MSc in Mechanical Engineering from Shiraz University of Technology, Iran in 2019. She is currently a PhD graduate in Shiraz University, Shiraz, Iran. Her research interests include theories of plates and shells and composite materials.

Farhad Abad received his BSc in Mechanical Engineering from Shiraz University, Shiraz, Iran in 2012. He also received his MSc and PhD in Mechanical Engineering from Shiraz University of Technology, Shiraz, Iran in 2014 and 2019, respectively. His research interests include computational mechanics, theories of plates and shells, and composite materials.

Li Li has been working as an Associate Professor at Huazhong University of Science and Technology since 2018. His research interests include multiscale modeling, nano-mechanics, structural dynamics, computational mechanics, and nanocomposites. He has published over 100 SCI papers with a sum citation of over 4900 times, and he was nominated as a highly cited researcher in the field of Engineering in 2019 and 2020. He is a reviewer for over 50 international journals and a book reviewer for some publishers. He is an Associate Editor of "Journal of Applied and Computational Mechanics" and "Frontiers in Mechanical Engineering", and an Editorial Board Member of "Archive of Applied Mechanics", and "Nanoscience & Nanotechnology-Asia".